Master's thesis

NTNU
Norwegian University of Science and Technology
Faculty of Information Technology and Electrical Engineering
Department of Electric Power Engineering

Erik Seeger Bjørnerem

Analyzing optimal sizing and operation of renewable hydrogen systems

Master's thesis in Energy and Environmental Engineering
Supervisor: Magnus Korpås
July 2021

NTNU
Norwegian University of Science and Technology

Erik Seeger Bjørnerem

Analyzing optimal sizing and operation of renewable hydrogen systems

Master's thesis in Energy and Environmental Engineering
Supervisor: Magnus Korpås
July 2021

Norwegian University of Science and Technology
Faculty of Information Technology and Electrical Engineering
Department of Electric Power Engineering

NTNU
Norwegian University of
Science and Technology

Preface

This thesis is the second of two mandatory theses for the degree Master of Science at the Norwegian University of Science and Technology. The work presented in this thesis is a continuation of the project thesis submitted in the fall of 2020 with the title "Optimal dimensioning of isolated, renewable hydrogen systems for integrating wind and solar power". This work has been an exciting challenge and I have learned a lot from these past months that I plan to incorporate in my future career.

I want to thank my fellow classmates for providing an arena for socialization in these otherwise restrictive times due to covid-19. Thereafter, I would like to thank Aftenposten for publishing their daily quiz. This has been an important daily ritual, second only to the excitement of checking out the the daily updates of covid-infections in Trondheim. What a time to be alive! I would like to thank my family for contribution towards finalizing the thesis. Last but not least, I would like to thank my supervisor Magnus Korpås for helping me along the way and sparking newfound inspiration when all else seemed hopeless.

Abstract

In order to reach net-zero carbon emissions by 2050 as agreed upon in the Paris agreement, the installed capacities of variable renewable energy (VRE) production is rapidly increasing. An increasing share of VRE generation leads to lower CO_2 emissions, but the inherent uncertainty and variability of renewable energy sources can pose significant operational challenges in today's power systems. In order to provide flexibility, electric energy storage (EES), hydrogen energy storage (HES) and external transmission can be utilized to provide regulatory means for higher VRE integration.

A least-cost capacity expansion model (CEM) is defined to determine the optimal system dimensions of a system containing electric load, hydrogen load, thermal generation, VRE generation, EES, HES and limited grid transmission. The operation of this optimal system is then analyzed using AC power flow (ACPF). If bus voltage constraints are violated, the CEM is reoptimized with additional constraints on system operation. The new optimal system operation is reanalyzed with ACPF, and this process is repeated until a valid system operation is obtained. This process was applied to the Leka power system through different case studies. The cases examined are a) a system with limited transmission capacity, b) a system without transmission, and c) a 100% renewable isolated system.

The results show solid incentives for VRE integration, and the CEM heavily favours wind power investments. In this case, wind power is cost-effective without subsidization, and the levelized cost of energy (LCOE) of wind power was 39.1 \$/MWh compared to the average spot price of 47.38 \$/MWh. The operation of this system featured maximum voltage deviations of 8% and line losses of 6.9% of total energy production. When wind power is replaced by solar power, the annual cost of operation is increased by five times due to the investment of a large EES. This system featured maximum voltage deviations of 19% and line losses equalling 9.8% of the total power generation. Due to violating voltage restrictions, this case was reoptimized, and the new solution featured similar system dimensions but significantly smoother production scheduling.

Through analysis of defined case studies, it was found that the capacity of the HES varies with the flexibility in the system. For the case with grid transmission, the HES capacity is one day of hydrogen load demand. When the transmission line is removed, the capacity is increased to 3 days as there are periods with low VRE production. Additionally, when the thermal generator is removed, the capacity is increased to 6 days. The cost of the fuel cell proved too high in order to activate the fuel cell investment.

In conclusion, the least-cost optimal systems feature the largest VRE integration when grid transmission is included. This way, surplus VRE production can be exported for revenue, and power import can be utilized in periods with low VRE generation. However, this lead to increased power flows which caused a larger deviation in voltage levels.

Keywords: capacity expansion model, power systems operation, power flow analysis, variable renewable energy, flexibility, hydrogen storage

Sammendrag

For å nå netto-null karbonutslipp innen 2050, som avtalt i Paris-avtalen, ser man en markant økning av installert effekt fra fornybar energiproduksjon. Ved bruk av økt fornybar energiproduksjon går utslipp av CO_2 ned, men usikkerhet og variasjon i produksjon kan føre til utfordringer knyttet til balansering av last og produksjon i drift av dagens kraftsystemer. For å utnytte fornybar energiproduksjon i større grad kan elektrisk energilagring (EES), hydrogenlagring (HES) og nettoverføring brukes til å skape fleksibilitet i kraftsystemet for å balansere produksjon og forbruk.

En kostnadsminimerende kapasitetsutvidelsesmodell (CEM) er definert for å bestemme den optimale størrelsen av komponenter i et system som inneholder elektrisitetsforbruk, hydrogenforbruk, termisk energiproduksjon, fornybar energiproduksjon, EES, HES og begrenset nettoverføring. Drift av dette optimale systemet blir deretter analysert ved hjelp av lastflyt. Dersom begrensninger for spenningsnivåer overskrides, blir CEMen optimert på nytt med ekstra driftsbegrensninger. Driften av det nye optimale systemet er så analysert igjen med lastflyt, og denne prosessen gjentas til en gyldig drift av systemet er oppnådd. Denne prosessen ble så testet for kraftsystemet på øyen Leka for ulike scenarioer. De ulike scenariene er a) et system med begrenset overføringskapasitet, b) et system uten overføring og c) et 100 % isolert fornybart system.

Resultatene viser tydelige beslutninger for å integrere en større andel fornybar energiproduksjon, spesielt vindkraft. Selv uten subsidier er vindkraft konkurransedyktig med annen energiproduksjon og har en levetidsenergikostnad (LCOE) på 313 NOK/MWh sammenlignet med gjennomsnittlig spotpris på 379 NOK/MWh. Lastflytsanalysen viser et spenningsavvik på 8 % og linjetap på 6,9 % av total energiproduksjon. Når vindkraft erstattes av solenergi, økes de årlige driftskostnadene med fem ganger på grunn av ett større lagringsbehov. Denne løsningen hadde spenningsavvik på 19 % og linjetap tilsvarende 9,8 % av total kraftproduksjon. Ettersom spenningsrestriksjonene ble brutt, ble det gjennomført en ny optimal dimensjonering og lastflyt. Den nye løsningen inneholdt komponenter av lignende størrelse, men kraftproduksjon var nå betydelig jevnere.

Analyse av de definerte casestudiene viste en sammenheng mellom størrelsen på hydrogenlageret og fleksibiliteten i systemet. I tilfellet med nettoverføring kan hydrogenlageret dekke en dag hydrogenforbruk. Når overføringslinjen fjernes økes størrelsen på lageret til 3 dagers forbruk ettersom det oppstår perioder med lav fornybar energiproduksjon som ikke kan dekkes med import lengre. Når så den termiske generatoren også fjernes, økes størrelsen til 6 dagers forbruk. Det var ingen tilfeller hvor det lønte seg å investere i brenselsceller for ekstra kraftproduksjon ettersom kostnaden av denne komponenten var for dyr i forhold til bruken.

Avslutningsvis viser de kostnadsoptimale systemene at nettoverføring gir størst mulighet for investeringer av fornybar energiproduksjon. Overskuddsproduksjon fra fornybare energikilder kan eksporteres og selges, samt at forbruket kan dekkes av import i perioder med lav fornybarproduksjon. Et rent fornybart system førte til store kraftoverføringer som ga større avvik i spenning.

Contents

List of Figures

List of Tables

Nomenclature

Abbreviations

ASFC	Annual specific fixed cost
BESS	Battery energy storage system
CEM	Capacity expansion model
LCOE	Levelized cost of energy
O&M	Operation and maintenance
PF	Power flow
SCC	Specific capital cost
SoC	State of charge
ts	Time series

Indices

d	Demand
e	Electric Energy Storage (EES)
eh	Electrolyzer
exp	Export in transmission line
fh	Fuel cell
g	(Thermal) generator
h	Hydrogen Energy Storage (HES)
imp	Import in transmission line
l	(Transmission) line
s	Load shedding
t	Hour in a year
v	Variable Renewable Energy (VRE)

Parameters

η_i	Efficiency of component i

$\overline{P_{gi}}$ Upper limit on real power generation in generator i

$\overline{Q_{gi}}$ Upper limit on reactive power generation in generator i

$\overline{U_i}$ Upper limit on voltage magnitude in bus i

$\underline{U_i}$ Lower limit on voltage magnitude in bus i

AF_i Availability factor of resource i

$C_{exp,t}$ Discrete export power cost for in \$/MWh

$C^l_{exp}(t)$ Continuous export power cost for line l in \$/MWh

$C_{imp,t}$ Discrete import power cost for in \$/MWh

$C^l_{imp}(t)$ Continuous import power cost for line l in \$/MWh

F_i Annualized fixed investment cost in \$/kW or \$/kWh

$H_d(t)$ Continuous hydrogen demand in MW

$H_{d,t}$ Hydrogen demand in MW in hour t

$OM_{i,fixed}$ Fixed operation and maintenance cost of component i in \$/(kW year)

$OM_{i,var}$ Variable operation and maintenance cost of component i in \$/(kWh year)

SCC_i Specific capital cost of component i in \$/kW

V_i Variable production cost in \$/MWh

Variables

δ_i Voltage angle on bus i

$\overline{E_i}$ Storage capacity for storage i in MWh

$E_i(t)$ Continuous storage level for storage i in MWh

$E_{i,t}$ Storage level for storage i in hour t in MWh

E_{i0} Initial storage capacity for storage i in MWh

P_{gi} Real power generation from generator i

$q_i(t)$ Continuous power production/power flow from component i in MW

q_i, t Discrete power production/power flow in the hour t from component i in MW

Q_{gi} Reactive power generation from generator i

U_i Voltage magnitude on bus i

x_i Installed capacity of component i in MW

Sets

E EES plants

G (Thermal) Generators

H HES plants including eh and fh

L Transmission lines

T Hours in a year

V VRE plants

Introduction

For each passing day, the reality of a global climate crisis becomes more evident. However, in 2016, 190 countries signed the Paris Agreement, a collaborative, international agreement on mitigating the global impact of climate change. In this agreement, each country pledged to take actions to reduce individual greenhouse gas emissions in order to keep the global increase in temperature this century well below $2^{c}irc$C, preferably 1.5°C [2]. Earlier in 2021, the International Energy Agency (IEA) published a report on the actions required to reach net-zero emissions by 2050, as stated in the Paris agreement. Their solution proposes extensive electrification of sectors like buildings, heating, transport and industry. The increased electricity demand is to be covered by an increased renewable generation with wind and solar power shares varying from 15-80% of total generation capacity for 2050 [3].

Integrating variable renewable energy (VRE) production provides clean, renewable energy that can replace carbon-based generation. VRE resources are replenished short-term and will never run out compared to fossil fuels. However, VRE generation is non-dispatchable and directly dependent on certain weather conditions. This insecurity can lead to challenges in balancing generation and load demand in a system due to the intermittent availability of VRE. Norway has a traditional top-down power grid topology with decreasing transmission further from the main grid. Remote locations with excellent wind conditions may struggle to integrate VRE generation due to lacking transmission capacity. In order to ensure load balance, the flexibility of energy storage could be implemented.

Instead of dumping surplus VRE generation, this can be stored in electric energy storage (EES) or hydrogen energy storage (HES). EES in batteries (BESS) features high roundtrip efficiency and is therefore favoured for short term storage. On the other side, hydrogen is energy-dense, and the cost of capacity for HES is meager compared to BESS. In a HES, hydrogen is extracted from water through energy-intensive electrolysis. This hydrogen can be stored in tanks and be used to cover flexible hydrogen load demand. Additionally, the stored hydrogen can be used in a fuel cell to generate electric power in periods with low VRE generation. The conversion of hydrogen to electric power and vice versa occurs at low efficiency, introducing large conversion losses in the HES. However, surplus VRE generation that would otherwise be dumped can be used to fill the HES over a long time period. A fuel cell can then be utilized for backup, featuring similar efficiency to a gas turbine with the same purpose.

In the IEA report, hydrogen is used as an energy carrier to cover up to 10% of the load demand [3]. Norway also has plans on incorporating hydrogen as an energy carrier, especially for use in the transport sector [4]. There are planned and completed projects replacing passenger ferries run on diesel are replaced by hydrogen ferries [5]. These ferries operate in coastal areas in Norway where wind conditions are excellent. As previously

found, the inclusion of flexible HES can provide better integration of VRE generation [6].

Previous work has presented operation analysis of wind hydrogen systems located in coastal Norway [1]. In this study, a logistic model was defined to maximize the utilization of available wind power and minimize the amount of hydrogen not supplied while maintaining valid system operation. Here the electrolyzer- and wind power capacity were set based on intuition instead of optimization. In the project thesis from December 2020, the writer presented work on optimal dimensioning of isolated, renewable hydrogen systems [6]. Here, the deterministic capacity expansion model (CEM) yielded optimistic and unrealistic system dimensions and scheduling. By combining the CEM with a power flow (PF) analysis, both internal transmission constraints and system operation can be validated for the optimal renewable system. Through this analysis, the writer hopes to bring further light to the question: "How does high VRE integration affect optimal system dimensions and system operation?"

In order to answer this question, the operation of optimal renewable systems set by the deterministic CEM is analyzed. If voltage violations or line overload occurs, the goal is to constrain the CEM further to get a more realistic optimal system with valid power flow operation. This goal is achieved by extending the least-cost CEM formulation to include additional operational constraints.

This process of answering the research question is split into two parts. Firstly, the CEM is defined using a least-cost linear program (LP) formulation. This model takes VRE availability, load demand and generation costs as input and outputs the optimal system dimensions and scheduling. After that, a PF analysis is performed on the optimal system scheduling to determine the feasibility and efficiency of the CEM scheduling. The process of setting optimal system dimensions and analyzing system operation is then exemplified through a case study of the Leka power system.

1 Theory

This section presents the theory on system specification, capacity expansion modelling and power flow calculation relevant to this thesis. In order to examine the problem formulation of the thesis, both a capacity expansion model (CEM) and a power flow (PF) formulation are presented. Firstly the system is defined with different components in section 1.1. Then the CEM is defined in section 1.2. The CEM is deterministic and sets the optimal system dimensions and scheduling in a system containing thermal generation, VRE production, BESS (Battery Energy Storage System), HES and external grid transmission. The solution to this capacity expansion problem will give the best investments for a given system to minimize annual costs. Lastly, an AC power flow problem is formulated in section 1.3. Based on the scheduling of power injection from the CEM, the solution to the PF problem gives power flows within a system and provides voltage magnitudes and power losses during system operation.

The work presented in section 1.1, section 1.2 and section 2.1 is heavily influenced by work from my project thesis submitted December 2020 [6]. The previous work is highly relevant for this thesis and is both extracted and extended to cover the scope of this thesis. This disclaimer is made to inform the reader that no intent of plagiarism is made, and inform the reader that it is not necessary to read the previous work to understand this thesis.

1.1 System specification

In a power system, there must be a balance of load and demand in order to maintain stability. The sum of power produced must therefore equal the sum of power consumed. A power system can be made up of multiple different production units as well as multiple load units. Internal system transmission capacity is assumed infinite, and all the load units can be combined to form a single load. The total load will then have to be supplied by all production units. If the power production does not cover the power demand, stored power can be utilized. Similarly, power can be stored at times with surplus power production. A power system with production and storage units is given in fig. 1.

The power generation and demand must be balanced in this system. The power flows are defined positive if they serve the load and negative if they flow in the opposite direction. By assuming zero internal impedance the power balance can be formulated:

$$P_{v1} + P_{v2} + P_g - P_{e-} + P_{e+} = P_d \tag{1}$$

Additionally, BESS balance can be expressed by the difference in charge and discharge powers.

$$\frac{dE_e(t)}{dt} = \eta_{e-} \cdot P_{e-}(t) - \frac{P_{e+}(t)}{\eta_{e+}} \tag{2}$$

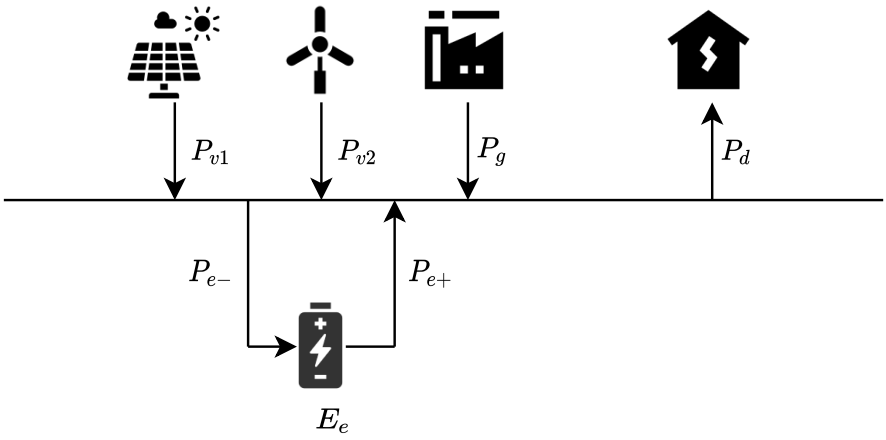

Figure 1: One line diagram of a power system with different types of energy production and BESS. Power production from solar, wind and thermal generators are denoted P_{v1}, P_{v2} and P_g. Battery charge and discharge is denoted respectively P_{e-} and P_{e+}. Battery charge level is given as E_e. Total system power demand is given as P_d.

Here η_{e-} is the charging efficiency, and η_{e+} is the discharge efficiency of the BESS. These efficiencies include the efficiency of an AC-DC converter as the BESS is operated in DC. The charge and discharge efficiencies can vary with different BESS technologies. Even though the round-trip efficiencies can be high, eq. (2) highlights the fact that energy is lost through charging and discharging a battery. In other words, the benefit of storing energy for later use also comes with the drawback of some energy loss.

In addition to BESS, the system can be expanded to include HES. Similarly to BESS, the HES can be "charged" by extracting hydrogen gas through water electrolysis. This hydrogen can be stored in tanks for a longer time compared to BESS plants such as batteries. HES units are more compact than BESS due to the high energy density of hydrogen. This is beneficial and saves weight if the HES is to be used on a vehicle, for example. Due to the high energy density of hydrogen, it makes an excellent energy carrier for energy-intensive services like transportation [7]. The stored hydrogen can also be converted back to electrical power in a fuel cell. The addition of a hydrogen loop is shown in fig. 2.

With the added hydrogen loop the power balance in eq. (1) must be updated to account for the power used for electrolysis and the power output of the fuel cell. From eq. (1) the new power balance equation becomes:

$$P_{v1} + P_{v2} + P_g - P_{e-} + P_{e+} - P_{eh} + P_{fh} = P_d \tag{3}$$

The BESS state of charge is unaffected by the addition of the hydrogen loop as these are decoupled. Similarly to BESS the HES balance can be expressed:

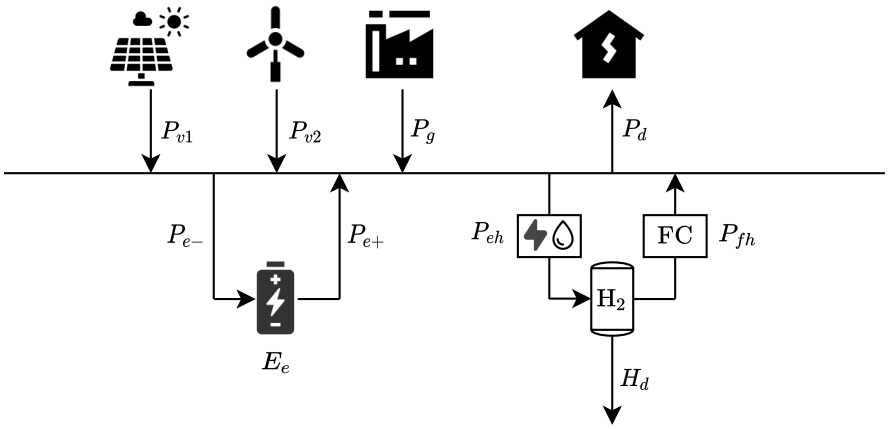

Figure 2: One line diagram of a power system with added electrolyzer, hydrogen storage and fuel cell. Power for water electrolysis is given as P_{eh}. Fuel cell output power is P_{fh} and the hydrogen storage level is given as E_h. H_d represents a hydrogen load.

$$\frac{dE_h(t)}{dt} = \eta_{eh} \cdot P_{eh}(t) - \frac{P_{fh}(t)}{\eta_{fh}} - H_d(t) \tag{4}$$

where η_{eh} is the the electrolyzer efficiency, η_{fh} is the fuel cell efficiency and H_d is a potential hydrogen demand. Similarly to the BESS, η_{eh} and η_{fh} also include the efficiency of an AC-DC converter as both the electrolyzer input and fuel cell output is DC power. The round-trip efficiency of the hydrogen storage is a lot lower than the BESS. However, hydrogen storage can be utilized as long term storage and provides additional flexibility to the BESS. Another benefit of hydrogen storage is that it can serve a hydrogen load. Hydrogen storage can therefore serve as a flexible resource both for electrical power demand and hydrogen demand.

Another source of flexibility to a local energy system is import and export. By connecting the power system to an external grid then power can be exchanged across different power systems. With this, surplus generation in one area can be used to cover load in another area. This way, the system prices are lowered, and the total surplus is increased. The system with included transmission capability is given in fig. 3.
Adding power import P_{imp} and power export P_{exp} to the load balance equation eq. (3) results in eq. (5). Here the transmission losses are assumed zero.

$$P_{v1} + P_{v2} + P_g - P_{e-} + P_{e+} - P_{eh} + P_{fh} + P_{imp} - P_{exp} = P_d \tag{5}$$

From this equation, it is evident that the import and export of power can balance mismatches in power generation and load demand. If power generation is expensive in an area, it is possible to cover all of the load merely by power import, given that the transmission capacity is sufficient.

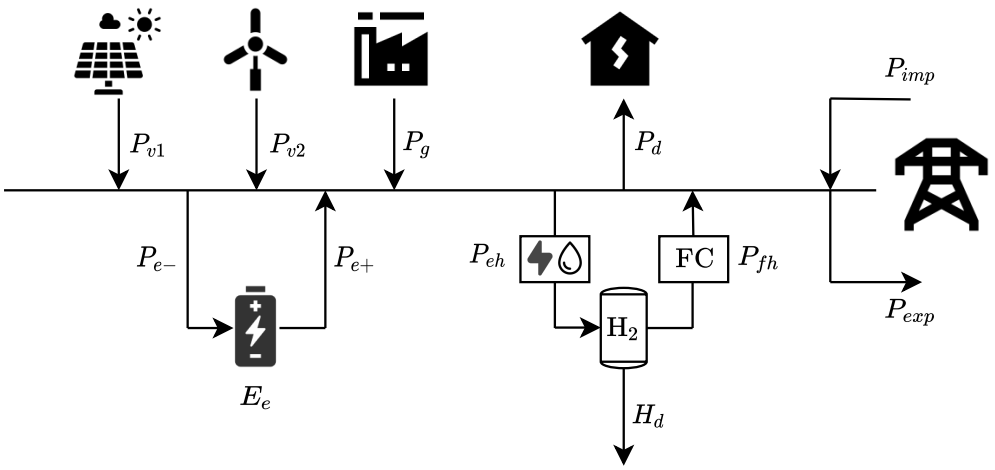

Figure 3: One line diagram of a power system with added transmission capacity for import and export of power. Import power is given as P_{imp} and export power is given as P_{exp}.

1.2 Capacity expansion models

As previously stated, the capacity of power production units and storage units must be chosen so that the load demand is covered at all times in order to maintain stable operation of the power system. The dimensioning of production units can be implemented in a large number of different combinations. One option would be to cover all load using thermal generators. This solution is predictable and provides great security of production scheduling but leads to high emissions and high variable costs. VRE plants have higher investment costs but have much lower operating costs. However, the uncertain nature of VRE production increases the need for energy storage in order to meet the demand in periods with low VRE production. VRE production availability varies based on geographic location, and therefore different locations will have different optimal system dimensions. Therefore, the optimal combination and dimensions of production and storage units are affected by different costs and VRE production capabilities in a given area.

A model that can find such an optimal solution must weigh the benefits and costs of plants against each other while also maintaining production and load balance. VRE availability can lead to challenges in load balancing, and demand-side flexibility can have a significant impact on the integration of VRE production [8]. This is a large topic by itself, and in order to limit the scope of this thesis, the load is assumed inflexible. The optimization problem can be formulated as a least-cost planning problem, where the annual costs are minimized while sufficiently covering a given load.

1.2.1 LP CEM for BESS

A least-cost capacity expansion problem for the system with BESS storage (fig. 1) is presented in a paper by Magnus Korpås and Audun Botterud [9]. This model is given by eq. (6a)-(6h) and contains the variables x_i and $q_i(t)$. Here x_i is defined as installed capacity for unit i and $q_i(t)$ represents power flow from unit i with positive direction towards the load. The variable $q_i(t)$ is time-variant, meaning the power flow can change for different time periods while x_i is time-invariant. The model is defined generally where the number of thermal generators, VRE plants and BESS plants are G, V and E respectively.

$$\min C = \sum_{g\in G}\left[F_g x_g + V_g \int_0^T q_g(t)dt\right] + \sum_{v\in V} F_v x_v + \sum_{e\in E}\left[F_e^{pwr} x_e + F_e^{en}\bar{E}_e\right] + V_s\int_0^T q_s(t)dt \tag{6a}$$

$$\text{s.t.} \sum_{g\in G} q_g(t) + \sum_{v\in V} q_v(t) + \sum_{e\in E}\left[q_{e+}(t) - q_{e-}(t)\right] + q_s(t) = q_d(t) \qquad \forall \quad t \tag{6b}$$

$$0 \leqslant q_g(t) \leqslant x_g \qquad \forall \quad g \in G, t \tag{6c}$$

$$0 \leqslant q_v(t) \leqslant AF_v(t)x_v \quad \forall \quad v \in V, t \tag{6d}$$

$$0 \leqslant q_{e+}(t) \leqslant x_e \qquad \forall \quad e \in E, t \tag{6e}$$

$$0 \leqslant q_{e-}(t) \leqslant x_e \qquad \forall \quad e \in E, t \tag{6f}$$

$$\frac{dE_e(t)}{dt} = \eta_{e-}\cdot q_{e-}(t) - \frac{q_{e+}(t)}{\eta_{e+}} \quad \forall \quad e \in E, t \tag{6g}$$

$$0 \leqslant E_e(t) \leqslant \bar{E}_e \qquad \forall \quad e \in E, t \tag{6h}$$

The objective function eq. (6a) minimizes the sum of annualized fixed costs ($F_i x_i$), annual variable thermal generation costs ($V_g \int_0^T q_g(t)$) and annual cost of load shedding ($V_s \int_0^T q_s(t)$). Here the integral from 0 to T represents an annual time period. Variable costs of VRE are set to zero as O&M costs are assumed negligible. BESS investment costs are linear functions of discharge capacity x_e and energy capacity $\bar{E}$. Equation (6b) states the instantaneous power balance and is similar to eq. (1) with added load shedding $q_s(t)$. Equation (6c)-(6f) state that the power output of each unit must be non-negative and at most equal to the installed capacity. For VRE units, the power output $q_v(t)$ is also bound by an availability factor $AF_v(t)$, which states how much of the installed capacity

can be utilized based on weather data. The BESS storage balance from eq. (2) is the same as eq. (6g). Lastly, eq. (6h) states that the BESS storage level must be non-negative and lower than the dimensioned energy capacity.

1.2.2 LP CEM for BESS and HES

In order to include hydrogen storage and conversion in the CEM, there are additional components that need to be added according to fig. 2. These are an electrolyzer, a hydrogen tank and a fuel cell. These three components make up the hydrogen loop, and the system could, in theory, have any number of these hydrogen loops with different dimensions. The set of such hydrogen loops in the system is denoted H. For each index in this set, variables x_{eh}, x_{fh} and $\bar{E}_h$ represent electrolyzer capacity, fuel cell capacity and hydrogen storage capacity respectively. Additional variables are $q_{eh}(t)$ and $q_{fh}(t)$ for electrolyzer power input and fuel cell power output.

The model can now be extended using these variables. The previous objective function (6a) now includes additional costs for the annualized fixed costs of the electrolyzer, storage capacity and fuel cell. This results in the new objective eq. (7a). In eq. (6b) electrolyzer power must be subtracted and fuel cell power must be added, resulting in eq. (7b). Equation (6c)-(6h) remain unchanged, but similarly to the BESS there needs to be added constraints for HES balance as well as upper limits to q_{eh} and q_{fh}. These are added in eq. (7i)-(7l). The only difference is that a hydrogen load is subtracted from the HES storage level for each timestep in eq. (7l). The complete extended least-cost capacity expansion problem is defined generally by eq. (7a)-(7l).

$$\min C = \sum_{g\in G}\left[F_g x_g + V_g \int_0^T q_g(t)dt\right] + \sum_{v\in V} F_v x_v + \sum_{e\in E}\left[F_e^{pwr} x_e + F_e^{en}\bar{E}_e\right] + V_s \int_0^T q_s(t)dt + \sum_{h\in H}\left[F_{eh}x_{eh} + F_{fh}x_{fh} + F_h^{en}\bar{E}_h\right] \quad (7a)$$

s.t.

$$\sum_{g\in G} q_g(t) + \sum_{v\in V} q_v(t) + \sum_{e\in E}\left[q_{e+}(t) - q_{e-}(t)\right] + \sum_{h\in H}\left[q_{fh}(t) - q_{eh}(t)\right] + q_s(t) = q_d(t) \qquad \forall \quad t \quad (7b)$$

$$0 \leqslant q_g(t) \leqslant x_g \qquad \forall \quad g \in G, t \quad (7c)$$

$$0 \leqslant q_v(t) \leqslant AF_v(t)x_v \quad \forall \quad v \in V, t \quad (7d)$$

$$0 \leqslant q_{e+}(t) \leqslant x_e \qquad \forall \quad e \in E, t \tag{7e}$$

$$0 \leqslant q_{e-}(t) \leqslant x_e \qquad \forall \quad e \in E, t \tag{7f}$$

$$\frac{dE_e(t)}{dt} = \eta_{e-} \cdot q_{e-}(t) - \frac{q_{e+}(t)}{\eta_{e+}} \quad \forall \quad e \in E, t \tag{7g}$$

$$0 \leqslant E_e(t) \leqslant \bar{E}_e \qquad \forall \quad e \in E, t \tag{7h}$$

$$0 \leqslant q_{eh}(t) \leqslant x_{eh} \qquad \forall \quad h \in H \tag{7i}$$

$$0 \leqslant q_{ef}(t) \leqslant x_{ef} \qquad \forall \quad h \in H, t \tag{7j}$$

$$\frac{dE_h(t)}{dt} = \eta_{eh} \cdot q_{eh}(t) - \frac{q_{fh}(t)}{\eta_{fh}} - H_d(t) \quad \forall \quad h \in H, \tag{7k}$$

$$0 \leqslant E_h(t) \leqslant \bar{E}_h \qquad \forall \quad h \in H, t \tag{7l}$$

The objective function eq. (7a) includes the parameters F_i and U_i. F_i is the specific annualized fixed cost of plant i and is expressed by:

$$F_i = \frac{r}{(1+r)^{L_i}} SCC_i + OM_{i,fixed} \tag{8}$$

where r is the discount rate, L_i is the lifetime of plant i, SCC_i is the specific capital cost of plant i and OM_i is the specific fixed O&M costs of plant i. The variable costs of the thermal generators are:

$$V_g = \frac{c_{fuel}}{\eta_g} + \frac{c_{\mathrm{CO}_2} \cdot e_g}{\eta_g} + OM_{g,var} \tag{9}$$

where c_{fuel} is the fuel cost, η_g is the generator efficiency, c_{CO_2} is the CO_2 price, e_g is the emission rate and $OM_{g,var}$ is the variable O&M costs. The variable cost of load shedding, V_s is set to a large value in order to penalize the objective function for uncovered load.

In the model, the annualized fixed costs are assumed linear. Variable costs are also assumed linear for the total capacity of the thermal generators. A possible extension would be to express the variable generator costs as a piecewise linear function. This would be more accurate, but this simplification is deemed sufficient due to the limited scope of this thesis. The result is a linear model which is easily solved and guarantees an optimal solution with the simplex algorithm. The LP formulation is relatively simple and is therefore applicable to a wide selection of potential cases.

1.2.3 LP CEM for BESS, HES and transmission

The CEM can also be extended to include the option of power import and export as shown in fig. 3. The previously described stand-alone grid can be connected to a larger grid through one or more transmission lines. The set of transmission lines is defined by L, and the index ij indicates the node the line is connected to and from. For each line $l \in L$ the power flow from node i to node j is given as q^l_{ij}. As power can flow both ways, the sign of q_{ij} can be both positive and negative. In order to define all variables as positive q_{ij} is expressed as the difference between power import and export: $q^l_{ij} = q^l_{imp}(t) - q^l_{exp}(t)$. Here $q^l_{imp}(t)$ is power imported in the system and $q^l_{exp}(t)$ is power exported. $\overline{T_l}$ represents the maximum transfer capacity of the line. Power is either imported at a variable cost of import $C^l_{imp}(t)$ or exported at a variable revenue $C^l_{exp}(t)$. Here the price of import and export is given by the area price in the connected area.

In order to include import and export of power, the objective function is updated, and transmission constraints are added. The previous objective function (7a) is extended to include the annual cost and revenue from import and export and is given in eq. (10).

$$\begin{aligned}\min C = \sum_{g\in G}\left[F_g x_g + V_g \int_0^T q_g(t)dt\right] + \sum_{v\in V} F_v x_v + \sum_{e\in E}\left[F^{pwr}_e x_e + F^{en}_e \bar{E}_e\right] \\ + V_s \int_0^T q_s(t)dt + \sum_{h\in H}\left[F_{eh}x_{eh} + F_{fh}x_{fh} + F^{en}_h \bar{E}_h\right] \\ + \sum_{l\in L}\Big[\int_0^T C^l_{imp}(t)q^l_{imp}(t)dt - \int_0^T C^l_{exp}(t)q^l_{exp}(t)dt\Big] \quad (10)\end{aligned}$$

Similarly to the objective function, the import and export power must be added to the load balance equation in eq. (5). Import power is added, and export power is subtracted from the LHS of eq. (7b). This results in:

$$\begin{aligned}\sum_{g\in G} q_g(t) + \sum_{v\in V} q_v(t) + \sum_{e\in E}\left[q_{e+}(t) - q_{e-}(t)\right] + \sum_{h\in H}\left[q_{fh}(t) - q_{eh}(t)\right] \\ + q_s(t) + \sum_{l\in L}\left[q^l_{imp}(t) - q^l_{exp}(t)\right] = q_d(t) \qquad \forall \quad t \quad (11)\end{aligned}$$

In addition to the constraints (7c)-(7l) the following transfer constraints are added to the model:

$$0 \le q^l_{imp}(t) \le \overline{T_l} \qquad \forall \quad l \in L, t \quad (12a)$$

$$0 \le q^l_{exp}(t) \le \overline{T_l} \qquad \forall \quad l \in L, t \quad (12b)$$

With the added transfer capabilities, the model can cover mismatches between production and demand through power import while exporting surplus power generation for revenue. This flexibility provides an opportunity for non-dispatchable VRE production as surplus renewable production provides revenue instead of being lost through curtailment. How the use of transmission compares to energy storage will be examined closer by examining systems with and without the option of power transmission.

1.3 AC power flow

AC power flow (also known as complex load flow) is widely used for the planning and operation of power systems. ACPF is used when system impedances and generator scheduling is known (except slack bus). The solution to the ACPF problem provides information on whether the system operation is feasible or not. The ACPF provides a steady-state solution of line loading, active/reactive generation, bus voltage levels, bus angles and line losses. These results can be compared to predefined limits on system operation to determine if voltage stability or line capacities are violated. In section 1.3.1 the load flow equations are presented, in section 1.3.2 the PF bus classification is explained and in section 1.3.3 methods for solving the ACPF is shown.

1.3.1 Load flow equations

Here the load flow equations are derived. The state variables to be solved from the load flow equations are complex bus voltages $U_i = |U_i|\angle\theta_i$ which consists of a voltage magnitude $|U_i|$ and an angle δ_i. Line currents are caused by a difference in bus voltage and flow based on line impedance as given by eq. (13) and eq. (14) for an n-bus system. Note that all parameters and sizes not denoted by the magnitude symbol |x| represent complex vectors.

$$\left[I_{\text{Bus}}\right] = \left[Y_{\text{Bus}}\right]\left[U_{\text{Bus}}\right] \tag{13}$$

$$\begin{bmatrix} I_1 \\ \vdots \\ I_i \\ \vdots \\ I_n \end{bmatrix} = \begin{bmatrix} Y_{11} & \dots & Y_{1i} & \dots & Y_{1n} \\ \vdots & \ddots & \vdots & & \vdots \\ Y_{i1} & \dots & Y_{ii} & \dots & Y_{in} \\ \vdots & & \vdots & \ddots & \vdots \\ Y_{n1} & \dots & Y_{ni} & \dots & Y_{nn} \end{bmatrix} \begin{bmatrix} U_1 \\ \vdots \\ U_i \\ \vdots \\ U_n \end{bmatrix} \tag{14}$$

Here the Y-bus elements are defined by eq. (15). The line admittance $y_{ik} = \frac{1}{z_{ik}}$ where z_{ik} is the line impedance.

$$Y_{ik} = \begin{cases} \sum_{j=1\dots n, j\neq i} y_{ij} & i = k \\ -y_{ik} & i \neq k \end{cases} \tag{15}$$

From eq. (14) the current injection in bus i is given by:

$$I_i = Y_{i1}U_1 + Y_{i1}U_2 + \cdots + Y_{ii}U_i + \cdots + Y_{in}U_n = \sum_{k=1}^{n} Y_{ik}U_k \tag{16}$$

Complex power injection into bus i is defined:

$$S_i = P_i + jQ_i = U_i I_i^* \tag{17}$$

Substituting eq. (16) into eq. (17) yields:

$$S_i = P_i + jQ_i = U_i \Big(\sum_{k=1}^{n} Y_{ik}U_i \Big)^* = U_i \sum_{k=1}^{n} Y_{ik}^* U_k^* \tag{18}$$

The bus voltages can be written as $|U_i|\angle\delta = |U_i|\mathrm{e}^{j\delta_i}$. Using the euler identity $\mathrm{e}^{j\delta} = \cos\delta + j\sin\delta$ the complex power injection equation eq. (18) can be split into real and complex power injections for all buses n:

$$P_i = |U_i| \sum_{k=1}^{n_b} |Y_{ik}||U_k| \cos(\delta_i - \delta_k - \theta_{ik}) \qquad \forall \quad i \in 1\dots n \tag{19a}$$

$$Q_i = |U_i| \sum_{k=1}^{n_b} |Y_{ik}||U_k| \sin(\delta_i - \delta_k - \theta_{ik}) \qquad \forall \quad i \in 1\dots n \tag{19b}$$

Here the power injections are given as the difference in generation and load at bus i according to:

$$P_i = P_{Gi} - P_{Li}$$
$$Q_i = Q_{Gi} - Q_{Li}$$

Equations 19 are called the load flow equations. In addition to PF these equations also show up in optimal power flow (OPF). The load flow equations contain unknown real and complex power injections P_i and Q_i for each bus $i \in 1\dots n$. Additionally there are n unknown $|U_i|$ and δ_i. Y_{ik} and θ_{ik} represent $n \,\mathrm{x}\, n$ nodal admittance parameter values calculated from line impedance. As there are $2n$ equations with $4n$ unknown variables $2n$ variables need to be specified in order to solve for the remaining $2n$ unknowns. This is further presented in section 1.3.2.

1.3.2 Bus classification

Buses in the power system are classified as a slack bus, generator (PV) bus or a load (PQ) bus. The slack bus sets the reference voltage level and bus angle $|V_{slack}| = 1.0$ p.u. and $\delta_{slack} = 0$. Generators operate at a specified voltage level and therefore both $|V_i|$ and P_i are known for PV buses. If there is no active load at a PV bus then $P_{PV} = P_{Gi}$. In load buses the real and complex power consumption are known and $P_{PQ} = -P_{Li}$ and $Q_i = -Q_{Li}$. These classifications are summarized in table 1.

Table 1: Bus classification for AC power flow.

Bus type	**Known variables**	**Unknown variables**
Swing/Slack bus	$\|V_i\|$, δ_i	P_i, Q_i
Generator bus (PV)	P_i, $\|V_i\|$	Q_i, δ_i
Load bus (PQ)	P_i, Q_i	$\|V_i\|$, δ_i

1.3.3 Methods for solving

When all buses are classified as one of the three bus types in table 1, the load flow equations feature $2n$ equations with $2n$ unknowns. These can now be solved without the need for further variable specifications. However, the load flow equations are nonlinear and can therefore not be solved variable substitution. The load flow equations can be solved through iterative methods such as the Gauss-Seidel method or the Newton-Raphson (NR) method. The latter is the most used and is described below.

The objective of the NR method is to calculate the state variables δ_i and $|U_i|$ that yield the power injections (LHS) of eq. (19). To do this the mismatch vector $x = \left[\, \Delta\delta; \Delta|U| \,\right]$ is calculated by:

$$\Delta x = \begin{bmatrix} \Delta\delta \\ \Delta|U| \end{bmatrix} = -J^{-1} \begin{bmatrix} \Delta P \\ \Delta Q \end{bmatrix} \tag{20}$$

Here $\left[\, \Delta P; \Delta Q \,\right]$ are called the mismatch equations:

$$\Delta P_i = -P_i + |U_i| \sum_{k=1}^{n_b} |Y_{ik}||U_k| \cos(\delta_i - \delta_k - \theta_{ik}) \qquad \forall \quad i \in 1 \dots n \tag{21}$$

$$\Delta Q_i = -Q_i + |U_i| \sum_{k=1}^{n_b} |Y_{ik}||U_k| \sin(\delta_i - \delta_k - \theta_{ik}) \qquad \forall \quad i \in 1 \dots n \tag{22}$$

and J is the Jacobian:

$$J = \begin{bmatrix} \frac{\partial \Delta P}{\partial \delta} & \frac{\partial \Delta P}{\partial |U|} \\ \frac{\partial \Delta Q}{\partial \delta} & \frac{\partial \Delta Q}{\partial |U|} \end{bmatrix}$$

In order to solve these equations, an initial guess x_0 is made. This can be a "flat start" where all $|U_i| = 1.0$ p.u. and δ_i are set to zero. Equation (21) is solved using this initial value of x. The system is linearized around x in order to obtain the new J and solve eq. (20) for Δx. Then the bus voltages and angles are updated $x_{i+1} = x_i + \Delta x$. This process is repeated iteratively until the mismatch is smaller than the predefined stopping criteria. This method and numerous others are implemented in the MATLAB package MATPOWER [10].

2 Case study presentation

A case study was performed on the power system of Leka in order to examine the optimal power system dimensions and operation for different cases. Leka is an island located off the coast of Trøndelag and has good wind conditions comparable to other coastline locations in Norway. The local distribution grid is connected to the main Norwegian grid through a 6.5 MVA subsea cable. This transmission line provides flexibility on demand for local energy production at Leka and can be utilized to cover peak load demand. The impact this flexibility poses on VRE integration is examined in scenarios where the optimal system is designed both with and without external grid transmission. Thereafter, system operation is evaluated for the local power system at Leka to examine if internal operation constraints are upheld for the optimal systems. These scenarios are formulated as different cases in section 2.4.

The goal of this case study was to examine the optimal dimensions of a renewable hydrogen system and to analyze how the optimal system scheduling upholds operational constraints. This process is split into multiple steps as shown in fig. 4. Firstly the CEM is optimized with input data for plant investment- and operation costs and VRE availability for the Leka power system. The CEM then outputs optimal dimensions for generation units and energy storages within the system. Additionally, the CEM outputs optimal hourly scheduling of generator production as well as charging and discharging of storages. Time series (ts) of power injection for each bus is taken as input to the ACPF. If the operational constraints in the PF are violated, the CEM is optimized again with additional operational constraints. The method provided in fig. 4 is similar to the implementation of a model predictive controller (MPC) where a system is optimized over a finite horizon and only the first time step is implemented. The next CEM solution alters system dimensions and scheduling in order to uphold the new operation constraints. Once the operational constraints are upheld, the optimal system dimensions and operation is found.

The maximum deviation on voltage levels is set to 15%. Additionally, a deviation of 10% can occur for at most 1% of a week [11]. If a system does not uphold these two requirements, additional limits on upper and lower bounds on power injection are added to the CEM.

By implementing such a scheme, the CEM remains linear, and PF is used to analyze system operation for each time step. In order to implement this scheme, some additional assumptions are made to the general CEM in section 2.1. Then input data for the CEM is given in section 2.2 and in section 2.3 for the ACPF. Thereafter, the different cases of the case study is presented in section 2.4.

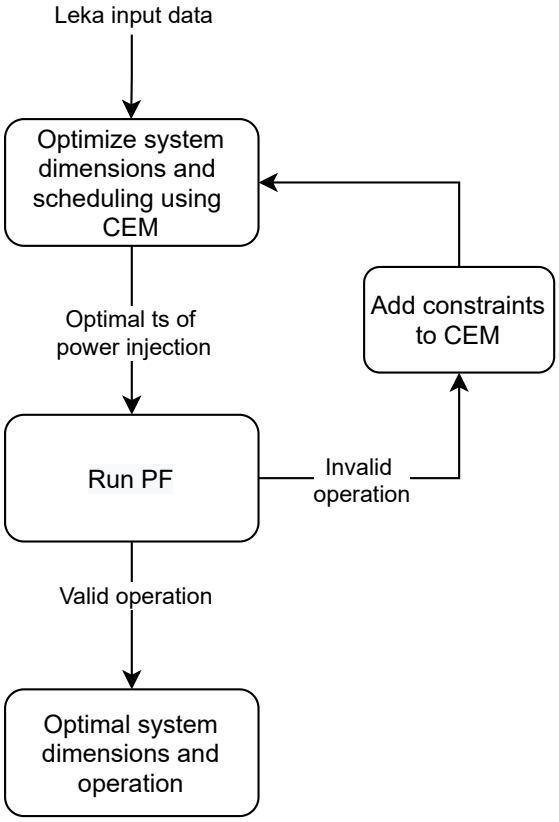

Figure 4: Flow chart describing how optimal system operation is evaluated using the CEM and PF in combination. The abbreviation ts is used for time series.

2.1 CEM assumptions

The general CEM is defined with continuous variables and parameters in eq. (7c)-(12). As the model minimizes annual cost the simulation period is set to one year with hourly time steps. The continuous variables and parameters are redefined as T=8760 hourly values over a year. The integrals in the objective function (10) can be reformulated according to eq. (23). In eq. (23) the index l is removed as there is only one transmission line in the Leka system. In addition equations (7c)-(7l), (11)-(12) must hold for all $t \in [1 \dots T]$.

$$V_g \int_0^T q_g(t)dt + V_s \int_0^T q_s(t)dt + \sum_{l \in L} \Big[\int_0^T C^l_{imp}(t) q^l_{imp}(t)dt - \int_0^T C^l_{exp}(t) q^l_{exp}(t)dt \Big] = V_g \sum_{t=1}^{T} q_{g,t} + V_s \sum_{t=1}^{T} q_{s,t} + \sum_{t=1}^{T} C_{imp,t} q_{imp,t} - \sum_{t=1}^{T} C_{exp,t} q_{exp,t} \quad (23)$$

The storage level equations for BESS (7g) and HES (7k) are updated for each time step. With an hourly time frame these equations can be reformulated to eq. (24) and eq. (25)

respectively. The initial storage levels are denoted $E_{e,0}$ and $E_{h,0}$ and are defined as variables rather than parameters. The CEM is then able to optimize the initial storage level at the start of the year. In order to avoid exploitation by emptying the initial storage content, eq. (24c) is added to ensure the end year storage levels surpass the initial storage levels.

$$E_{e,1} - E_{e,0} = \eta_{e-} \cdot q_{e-,1} - \frac{q_{e+,1}}{\eta_{e+}} \qquad \forall \quad e \in E \tag{24a}$$

$$E_{e,t} - E_{e,t-1} = \eta_{e-} \cdot q_{e-,t} - \frac{q_{e+,t}}{\eta_{e+}} \qquad \forall \quad e \in E, t \in [2 \dots T] \tag{24b}$$

$$E_{e,8760} \geq E_{e,0} \qquad \forall \quad e \in E \tag{24c}$$

$$E_{h,1} - E_{h,0} = \eta_{eh} \cdot q_{eh,1} - \frac{q_{fh,1}}{\eta_{fh}} - H_{d,1} \qquad \forall \quad h \in H \tag{25a}$$

$$E_{h,t} - E_{h,t-1} = \eta_{eh} \cdot q_{eh,t} - \frac{q_{fh,t}}{\eta_{fh}} - H_{d,t} \qquad \forall \quad h \in H, \quad t \in [2 \dots T] \tag{25b}$$

$$E_{h,8760} \geq E_{h,0} \qquad \forall \quad h \in H \tag{25c}$$

The modified CEM outputs optimal component dimensions for each component in the system and the optimal scheduling for each component to minimize the annual cost of operation. In order to complete the optimization, the CEM needs input data for fixed and variable costs regarding each system component. Additionally, the model needs electric and hydrogen demand profiles as well as profiles for VRE availability. Different cases can be defined by altering some of the input parameters and constraints, and the CEM gives the optimal system for each case. These optimal systems can be examined closer to compare how the component dimensions vary and how different means of flexibility affect the degree of VRE integration and total system annual costs.

2.2 CEM input data

Here the input data for the CEM is presented. The CEM requires time series for electric load demand, hydrogen load demand and VRE production availability at Leka. The optimal system at Leka is made up of the components shown in fig. 3. The components the model can invest in include a wind power plant, a solar power plant, a thermal plant (open cycle gas turbine), a BESS storage as well as an HES storage with a connected electrolyzer and fuel cell. The fixed and variable costs associated with each of these components are given in section 2.2.5.

2.2.1 Electric load demand

The annual electric load demand is shown in fig. 5 as described in a previous study at Leka [1]. The demand curve follows typical Norwegian conditions with higher demand during winter and lower demand during summer. Within a day, there are peaks in demand at around 8 in the morning and 20-21 in the evening. The maximum electric load demand is 1.26 MW, and the annual electric load demand is 7.27 GWh.

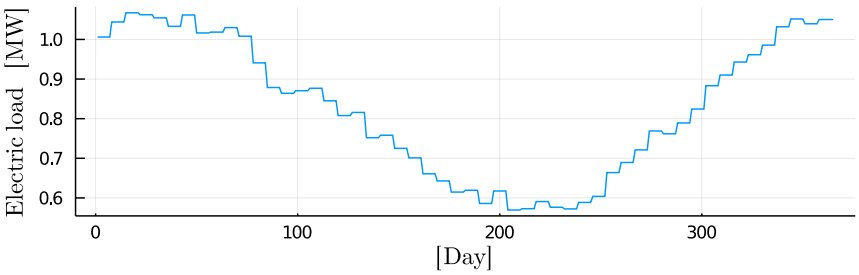

(a) Average daily electric load.

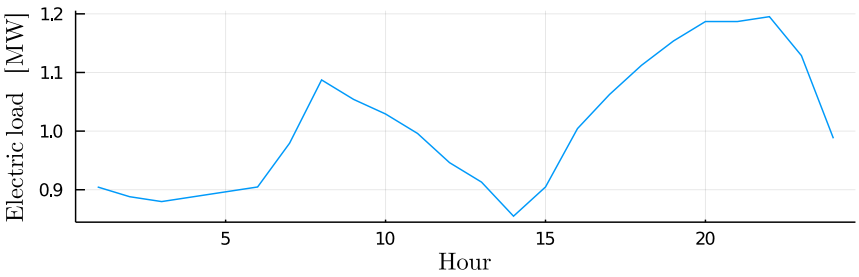

(b) Electric load variations during a day.

Figure 5: Variations in load demand for Leka. The daily variations in fig. 5(b) is given for the first day of the year. All other days follow the same pattern centered around the daily average electric load in fig. 5(a).

2.2.2 Hydrogen load demand

Similarly to previous studies, a hydrogen load is added to simulate a hydrogen ferry operating from Leka with an estimated daily hydrogen demand of 560 kg per day [1]. This demand is assumed constant during the year, and the hydrogen filling is scheduled at 06:00-07:00. The energy content of hydrogen is 33.3 kWh/kg [12]. The daily energy demand of hydrogen is then 18.66 MWh and 6.81 GWh annually solely to cover the hydrogen demand as shown in fig. 6. The peak hourly hydrogen demand is 18.66 MW as there is only one hour of demand daily. Hydrogen is converted through water electrolysis, and there is energy lost in the electrolyzer. Assuming an optimistic estimate of 75% efficiency in the electrolyzer [13] the annual electrolyzer consumption is about 9.08

GWh. The total annual energy demand in the Leka system is then about 16.35 GWh.

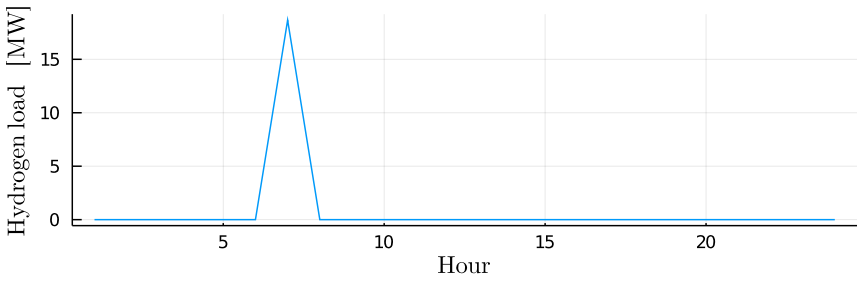

Figure 6: Daily hydrogen load demand for Leka. The hydrogen ferry is filled each day at 06:00-07:00.

2.2.3 VRE production availability

Production from VRE sources such as wind and solar power cannot be regulated upwards and are directly related to local weather conditions. The availability factors of VRE resources determine how much of the installed capacity can be utilized in a given time step on a scale from 0-100%. Data on the availability factors for wind and solar power production was collected from "Renewables.ninja". This website uses weather data from global reanalysis models and satellite observations [14] using methods described in [15] and [16]. Data from the GPS location of Leka (65.084772, 11.621566) yields the availability factors in fig. 7 based on data from 2019.

From fig. 7 it is clear that solar power production is greater in summer when the solar irradiance is higher. Solar power also varies daily in coherence with the rotation of the earth, which makes solar production easier to forecast. The availability factor of solar power peaks at 0.821 for a few hours but remains lower for most of the year. Wind power production is more fluctuant but provides more energy overall, especially in the winter months. The availability factor for wind peaks higher at 0.99 and is also higher than solar most of the year. The availability of wind and solar power can be further compared by plotting the cumulative availability as duration curves shown in fig. 8.

In fig. 8 the annual power production is much larger for 1 kW installed wind power than from 1 kW solar power. The duration curve for wind availability is almost linear, while solar availability is logarithmic. 1 kW of wind power yields a potential annual production of 3.80 MWh, while 1 kW solar power has a potential annual yield of 0.87 MWh. The potential yield from wind power is more than four times as large as that of solar power. The solar power plant also has zero production for half of the year due to a lack of irradiance at night. The CEM is therefore likely to invest in a larger share of wind power in this location. At the same time, wind power is less predictable, as seen in fig. 7,

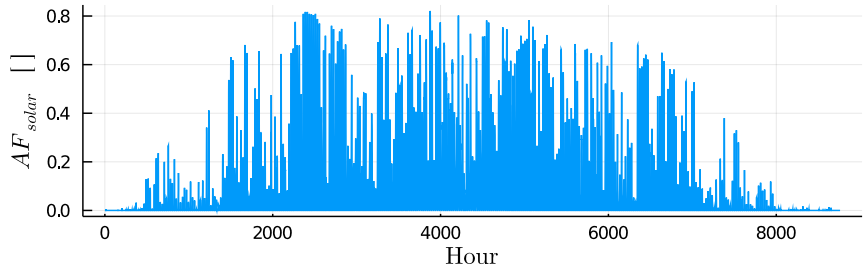

(a) Solar power.

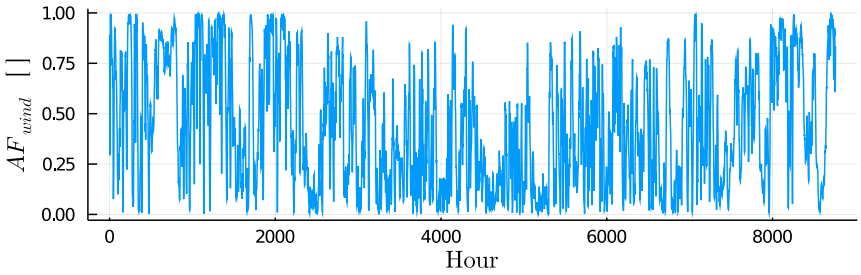

(b) Wind power.

Figure 7: Availability factors for wind and solar power during a year at Leka.

which would require some form of flexibility in order to avoid curtailment.

2.2.4 Spot price for import/export

Import and export of power add variable cost and revenue to the objective function in eq. (10). This power is bought and sold at an hourly day-ahead price set by pool trading at Nord Pool [17]. The Nordic countries are divided into different bidding areas, and Leka is located in NO3 (Trøndelag). Average daily power prices for the Trondheim area is shown in fig. 9 for the year 2019. For simplicity, the currency conversion $-NOK is assumed to be 8.0, which is close to the actual value in May 2021.

In fig. 9 the power prices are higher during winter and lower during summer. Here the spot price shows a similar pattern to the electric load demand curve (fig. 5(a)). This is due to supply and demand, and when the demand is high enough, more expensive generation is utilized like a gas turbine or diesel generator. These provide great flexibility but feature high costs and emissions. Over a year, the average power price is 47.38 $/MWh.

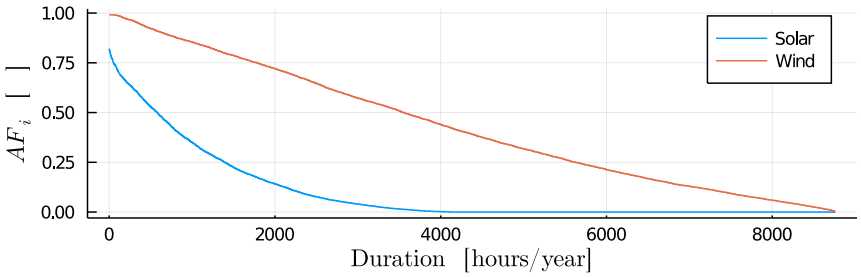

Figure 8: VRE availability duration curve for wind and solar power.

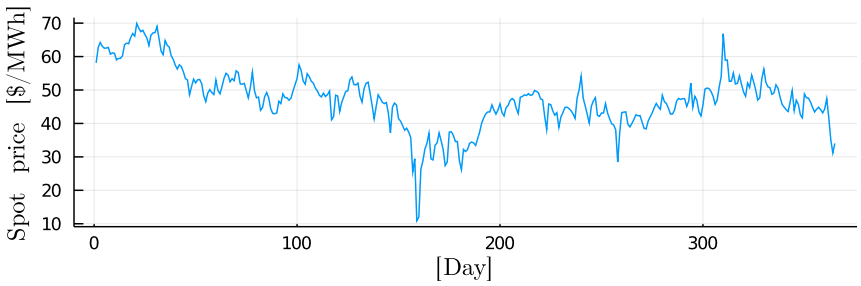

Figure 9: Average daily spot price for Leka (NO3) in $/MWh for 2019.

2.2.5 Parameters

The remaining input parameters for the CEM are fixed annual costs and variable costs of the different plants. These are calculated using eq. (8) and eq. (9) with the data given in appendix A. These costs are presented in table 2. The thermal generator is cheap, but the additional variable cost applies to each MWh produced. Another interesting note is that energy capacity for HES only costs one-sixth of the equivalent BESS. Bulk HES is cheaper per kWh, but both the electrolyzer and the fuel cell are more expensive than the BESS power interface.

Table 2: Specific annual fixed costs and variable costs for generator g, solar $v1$, wind $v2$, BESS e, shedding s electrolyzer eh, fuel cell fh and HES h. Calculated from costs in appendix A.

Parameter	**Value**	**Unit**
F_g	99.98	\$/kW/yr
V_g	104.36	\$/MWh
F_{v1}	94.08	\$/kW/yr
F_{v2}	146.53	\$/kW/yr
F_e^{pwr}	70.01	\$/kW/yr
F_e^{en}	21.62	\$/kWh/yr
V_s	3000.00	\$/MWh
F_{eh}	235.64	\$/kW/yr
F_{fh}	640.35	\$/kW/yr
F_h^{en}	1.452	\$/kWh/yr)

2.3 PF input data and assumptions

The PF problem can be formulated for the example system. A single line diagram of the 11 bus system at Leka is shown in fig. 10 with the different plants located at their respective bus. Bus 1 is defined as the swing/slack bus, and the external grid is simulated as a generator with infinite capacity. The wind power plant is connected to bus 10, while the electrolyzer, solar plant and BESS are located at bus 11. The plants connected at bus 11 all operate at DC power, and these are connected to bus 11 through a lossless inverter/rectifier station. The thermal plant is connected to the AC side of bus 11 in the cases where this is included.

The wind plant at bus 10 is connected to bus 9 through a transformer, increasing the voltage from 690 kV at the wind power side to 22 kV. Similarly, bus 11 is connected to bus 9 through a transformer that steps down the voltage from 22 kV to 400 V. The system also features distributed load at buses 3-9 according to table 3.

Table 3: Load distribution f_l for each load bus in the Leka system.

Bus	3	4	5	6	7	8	9
f_l	0.01	0.1	0.54	0.1	0.06	0.14	0.05

In some cases, the transmission line is removed. When this is the case, the slack bus would be cut off from the system and is therefore moved to bus 11. In the 100% renewable cases, there is assumed that slack power is supplied from BESS. However, this slack generation does not drain the BESS level as optimized by the CEM and can lead to some inaccuracies in net power balance. However, it is assumed that these cases will feature lower line losses, and therefore a lower need for slack utilization. Therefore this power imbalance should be insignificant.

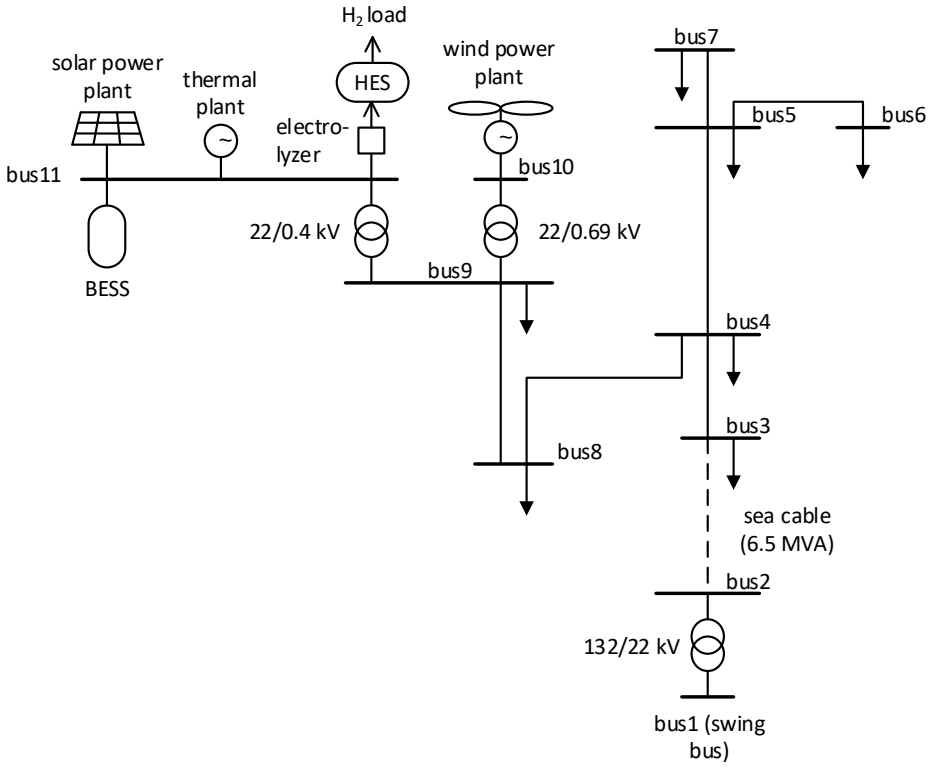

Figure 10: Single line diagram for Leka power system. Extended from [1] to include solar production, thermal generation a BESS.

2.3.1 Line data

The example system contains seven transmission lines and three transformers. The line data is given in table 4. The subsea cable (2-3) has the lowest transmission capacity, which makes it the bottleneck of the system in regards to power import and export. As the peak electric power demand is a lot lower than the line ratings, it is unlikely that any of the internal transmission lines will be congested.

2.3.2 Transformer data

The transformer data is given in table 5. Here the transformer rating S_N, primary and secondary voltage ratings and transformer impedance is given. The transformer rating at transformer 9-10 is given as 1.1 times the wind power plant capacity. The transformer rating at transformer 9-11 is given as 1.1 times electrolyzer + solar power rating. This is

Table 4: Line data for Leka system. L is line length, Z is line impedance, B is line susceptance and S_{max} is line rating.

Line	L [km]	Z [Ω/km]	B [µS/km]	S_{max} [MVA]
2-3	2.2	0.64 + j0.13	170	6.5
3-4	3.9	0.36 + j0.37	9.8	13.8
4-5	3.9	0.51 + j0.38	9.5	10.9
5-6	4.6	0.72 + j0.40	9.2	9.0
5-7	6.2	0.72 + j0.40	9.2	9.0
4-8	5.4	0.72 + j0.40	9.2	9.0
8-9	6.9	0.72 + j0.40	9.2	9.0

done to ensure that the transformers can handle system operation for systems of different VRE and electrolyzer dimensions.

Table 5: Transformer data. S_N is transformer rating, U_{N1} and U_{N1} are primary and secondary side voltage rating, e_r is transformer resistance and e_x is transformer reactance. For * and ** The transformer rating is given as 1.1 times the value of wind power plant rating and electrolyzer rating. For the cases including solar power the transformer rating of 9-11 is increased by 1.1 times the solar capacity.

Transformer	S_N [MVA]	U_{N1} [kV]	U_{N2} [kV]	e_r [p.u.]	e_x [p.u.]
1-2	12	132	22	0.004	0.086
9-10	*	22	0.69	0.009	0.055
9-11	**	22	0.4	0.011	0.047

The real power injection in each generator bus is set by the generator production. At bus 9, injected power is from wind power. At bus 11, multiple plants inject and consume power. The net real power injection is therefore $P_{11} = P_{v1} - P_{ch} + P_{dch} - P_{eh}$, where P_{v1} is solar plant production, P_{ch} is BESS charging power, P_{dch} is BESS discharge power and P_{eh} is electrolyzer power. Power factors of electrical load and VRE injection is set to 0.95 and 0.96 respectively.

The PF model outputs a steady-state solution for bus voltage, voltage angle and line loss in a single time step. The PF requires input for load demand, wind power production, solar power production and electrolyzer power for each time step. These active power injections are allocated to the correct bus according to fig. 10, and the power flow is calculated. The resulting voltage magnitudes indicate if the optimal system operates within the specified voltage limits. The system losses show the system efficiency and can be compared between different cases.

2.4 Cases

The example system is optimized for multiple cases to examine the effect of modifying specific input parameters. The modifications made feature changing certain costs and adding specific restrictions. The individual case results can then be examined, and optimal system dimensions and operation can be compared.

There are defined two cases for further inspection. These contain the subcases 1.1, 1.2, 1.3, 2.1 and 2.2, and an overview of these are given below. The first case is considered the base case, where the system is optimized without further changes or constraints (case 1.1). Thereafter, a similar system but without the transmission is defined for case 1.2. Lastly, the thermal generator is removed as well to create a 100% renewable system in case 1.3.

In the base case, wind power proved to be heavily favoured. Therefore a second case was defined to examine the effects of adding restrictions on wind power. Firstly, case 2.1 replaces wind power with solar power. This was implemented by forcing solar power to cover the same amount of energy produced by wind power in the base case (case 1.1). After that, case 2.2 features fully subsidized solar power to force out wind power investments and examine the operation of a system merely run by solar power. By fully subsidized it is meant that the investment cost SCC_{v1} and fixed O&M costs $OM_{v1,fixed}$ are set to 1 \$/kW and 1 \$/kW/yr respectively. Additionally, the transmission line and thermal generator were removed, similar to case 1.3. The overview of the cases is given:

Case 1.1: Base case as presented in section 1 and section 2.

Case 1.2: Base case with transmission capacity removed. Stand-alone system.

Case 1.3: Base case with transmission capacity and thermal generator removed. 100% renewable stand-alone system.

Case 2.1: The wind power plant is removed, and solar power is set to cover wind energy production from the base case.

Case 2.2: Solar power is fully subsidized (1 \$/kW and 1 \$/kW/yr). The constraint on wind power is removed as the cost reduction of solar should be large enough to force the CEM only to invest in solar power. Transmission capacity and thermal generation are removed. 100% renewable stand-alone system.

Based on the assumptions presented, some cases are more closely linked. Case 1.1 and 2.1 show how VRE generation can be utilized in a power system connected to the main grid and can be compared for wind (1.1) and solar (2.1). Cases 1.1, 1.2 and 1.3 feature changes in optimal system dimensions as more options for flexibility are removed. Lastly, the only difference between cases 1.3 and 2.2 is the lower cost of solar power in case 2.2. These cases can be compared to provide results on how sensitive the optimal system dimensions are to a change in solar power cost.

2.5 Model implementation

The CEM is implemented in Julia using the JuMP package for optimization. This package allows for a problem formulation featuring high level algebraic syntax [18]. The original LP formulation for EES from [9] is extended to include HES and transmission capacity. The Julia language provides high performance for fast computation, especially when used with the Gurobi solver.

The PF formulation is implemented in MATPOWER, a toolbox for MATLAB [10]. The standard formulation of ACPF, "runpf", is modified to take additional inputs on system load, electrolyzer power, fuel cell power and wind power generation [1]. In this thesis the formulation is further extended to include solar power generation, BESS charging and discharging. The modified PF implementation is run using data on power injections from the CEM for each hour of the year.

3 Results

In this section the results from the CEM and PF calculations are presented. From the CEM optimal system dimensions are given in section 3.1, annual energy balance is given in section 3.2 and the optimal production and storage schedules are given in section 3.3. Then the PF results are presented in section 3.4. Thereafter a sensitivity analysis is presented in section 3.5. The results presented in this section are then further analyzed in section 4.

Of the five cases only case 2.1 had invalid system operation as described in fig. 4. For this case the CEM was reoptimized with added operational constraints and these results are presented as "Case 2.1 rerun" and is compared to the five other cases.

3.1 Optimal system dimensions

The optimal system dimensions set by the deterministic CEM is presented in this subsection. The mix of components available are presented in fig. 3 and include a thermal plant, a wind plant, a solar plant, an BESS, an HES, a electrolyzer and a fuel cell. Additionally the initial SoC for both BESS and HES, $E_{e,0}$ and $E_{h,0}$ is considered a part of the optimal system dimensioning. The investment cost of components and operational costs add up to an annual operation cost C which is given for each case. The optimal systems for case 1.1, 1.2 and 1.3 are presented in table 6 and similarly cases 2.1 and 2.2 are presented in table 7.

Table 6: Base case optimal plant dimensions and objective function value C for each case. The indices are generator g, solar power $v1$, wind power $v2$, BESS e, electrolyzer eh, fuel cell fh and HES h. The unit of each variable is given in the last column.

Variable	**Case 1.1**	**Case 1.2**	**Case 1.3**	**Unit**
x_g	0	1.11	0	MW
x_{v1}	0	0.45	1.76	MW
x_{v2}	9.66	3.72	6.04	MW
x_e	0	0	0.92	MW
$\bar{E}_e$	0	0	10.32	MWh
$E_{e,0}$	0	0	5.05	MWh
x_{eh}	1.04	1.32	1.67	MW
x_{fh}	0	0	0	MW
$\bar{E}_h$	17.89	54.22	119.05	MWh
$E_{h,0}$	13.22	36.09	47.91	MWh
C	0.72	1.51	2.04	M$

Table 7: Case 2 optimal plant dimensions and objective function value C for each case. The indices are generator g, solar power $v1$, wind power $v2$, BESS e, electrolyzer eh, fuel cell fh and HES h. The unit of each variable is given in the last column.

Variable	**Case 2.1**	**Case 2.1 rerun**	**Case 2.2**	**Unit**
x_g	0	0	0	MW
x_{v1}	41.40	41.41	34.78	MW
x_{v2}	0	0	4.67	MW
x_e	11.56	11.56	0.98	MW
$\bar{E}_e$	66.15	66.12	10.03	MWh
$E_{e,0}$	66.15	66.12	4.29	MWh
x_{eh}	2.35	2.35	1.40	MW
x_{fh}	0	0	0	MW
$\bar{E}_h$	21.58	21.58	117.08	MWh
$E_{h,0}$	21.58	21.58	40.08	MWh
C	5.97	5.98	1.68	M$

3.2 Energy balance

In this subsection the annual energy balance is presented. The energy produced from each individual plant needs to cover both the electric load demand and hydrogen load demand. The annual production scheduled for each plant is shown in table 8 for case 1 and in table 9. Here electric energy demand and hydrogen demand are given as total energy demand. The tables also show conversion loss for energy storage and the total VRE curtailment which is the unused potential of installed VRE capacity.

The conversion loss gives the loss through charge and discharge of the BESS. The system also has conversion loss from water electrolysis of 2.27 GWh annually in order to serve the hydrogen load demand. As this is constant for all cases it does not show the difference between cases and is included in total energy demand rather than conversion losses in tables 8 and table 9.

Table 8: Base case annual energy production for each plant in the optimal solution. Energy loss represents energy lost through storage roundtrip efficiency. Loss due to thermal generator efficiency is not included. Load shedding is not considered energy production but rather the portion of the load one rather pays to not have to deliver.

Energy production	**Case 1.1**	**Case 1.2**	**Case 1.3**	**Unit**
Generator	0	3.99	0	GWh
Solar	0	0.47	1.57	GWh
Wind	36.21	11.90	14.97	GWh
Shed	0	0	0.05	GWh
Import	18.68	0	0	GWh
Export	38.54	0	0	GWh
Sum	16.35	16.35	17.00	GWh
Energy demand	16.35	16.35	16.35	GWh
Conversion loss	0	0	0.65	GWh
VRE curtailment	0.45	2.26	8.31	GWh

Table 9: Yearly energy produced in MWh by different plants in the optimal solution for each case. Energy loss represents energy lost through storage roundtrip efficiency. Loss due to thermal generator efficiency is not included. Load shedding is not considered energy production but rather the portion of the load one rather pays to not have to deliver.

Energy production	**Case 2.1**	**Case 2.1 rerun**	**Case 2.2**	**Unit**
Generator	0	0	0	GWh
Solar	36.21	36.21	6.30	GWh
Wind	0	0	10.36	GWh
Shed	0	0	0.06	GWh
Import	20.05	20.02	0	GWh
Export	36.65	36.80	0	GWh
Sum	19.61	19.43	16.71	GWh
Energy demand	16.35	16.35	16.35	GWh
Conversion loss	3.26	3.08	0.36	GWh
VRE curtailment	8.87	8.87	38.94	GWh

3.3 Optimal production scheduling

In this subsection the theoretical optimal scheduling of the CEM is presented. The time series for plant production and storage levels are given for each case in fig. 21-25. The cases with transmission also include import and export power time series. By sorting the time series duration curves are plotted for power production and transmission in fig. 11-15. The area under these curves add up to the annual energy production given in table 8 and 9. Similar duration curves of SoC are given in fig. 16-20.

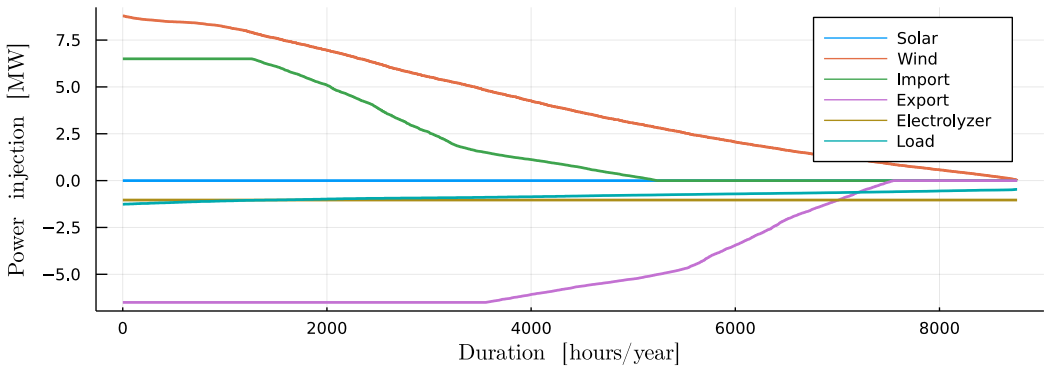

Figure 11: Duration curve of optimal system scheduling for case 1.1.

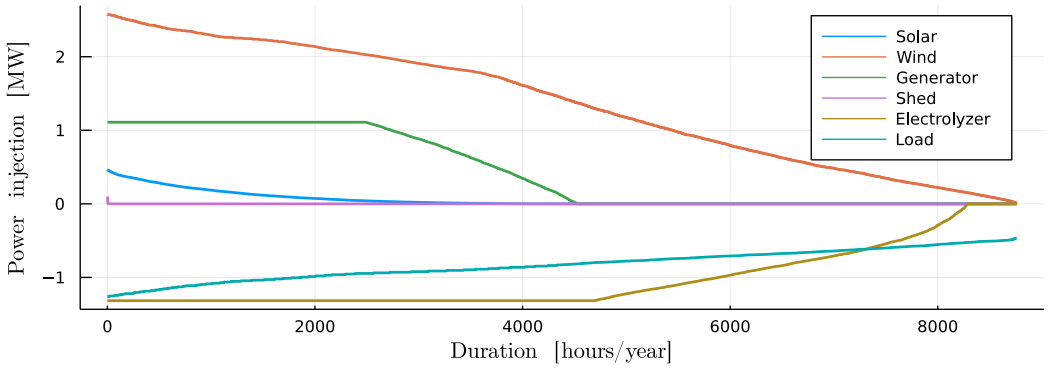

Figure 12: Duration curve of optimal system scheduling for case 1.2.

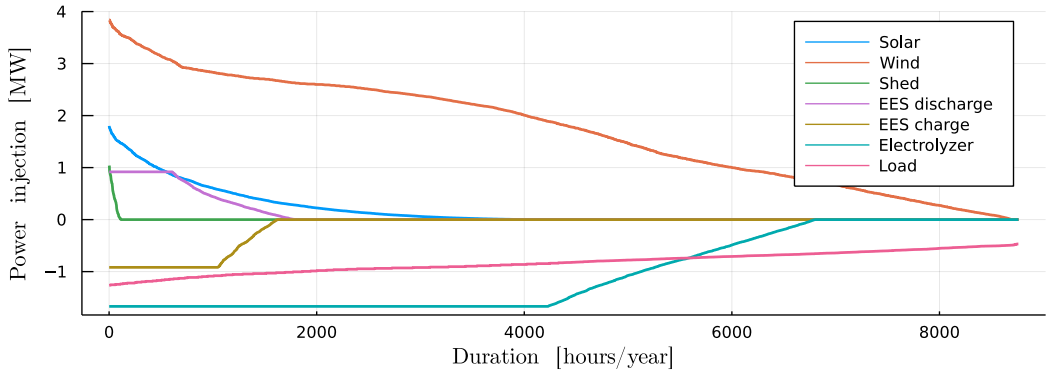

Figure 13: Duration curve of optimal system scheduling for case 1.3.

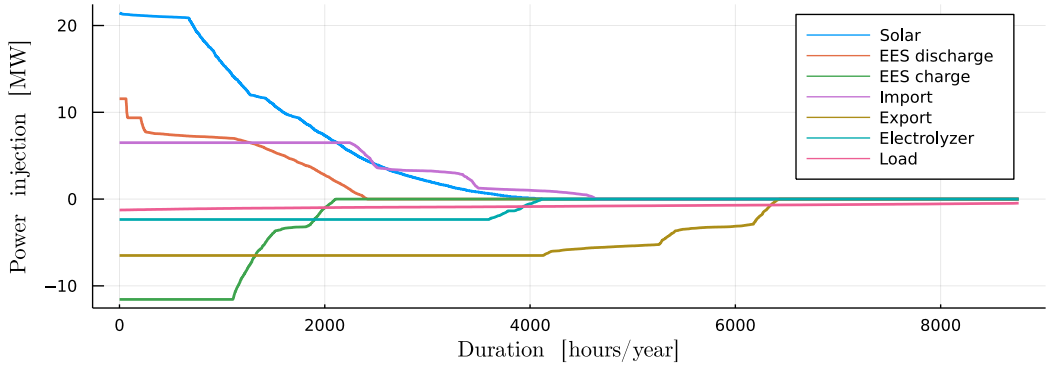

Figure 14: Duration curve of optimal system scheduling for case 2.1.

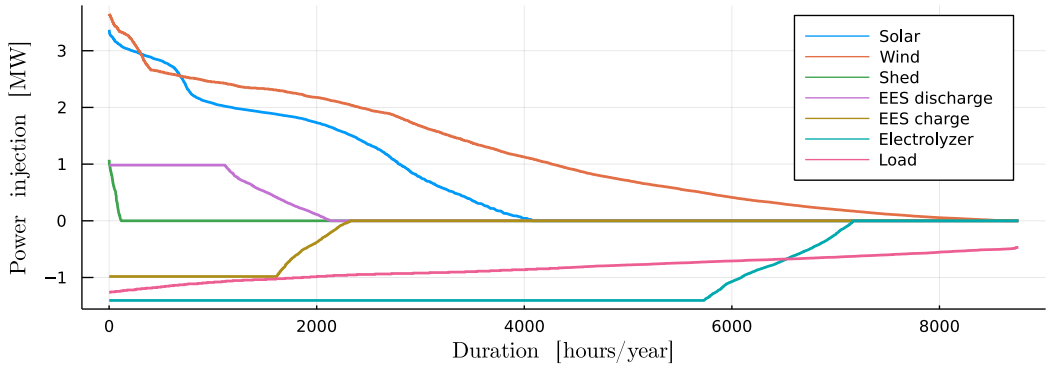

Figure 15: Duration curve of optimal system scheduling for case 2.2.

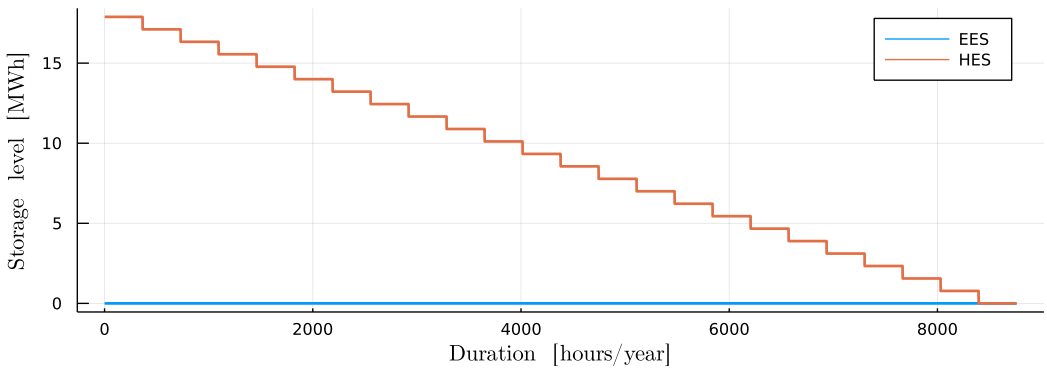

Figure 16: Duration curve of storage levels in case 1.1.

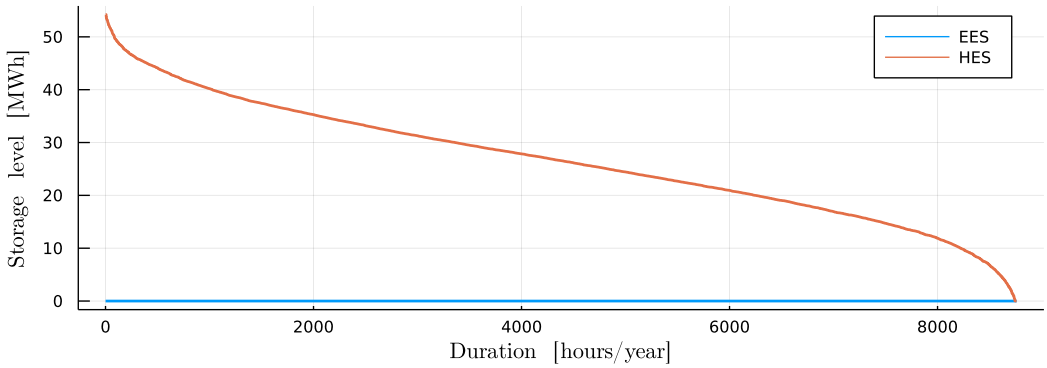

Figure 17: Duration curve of storage levels in case 1.2.

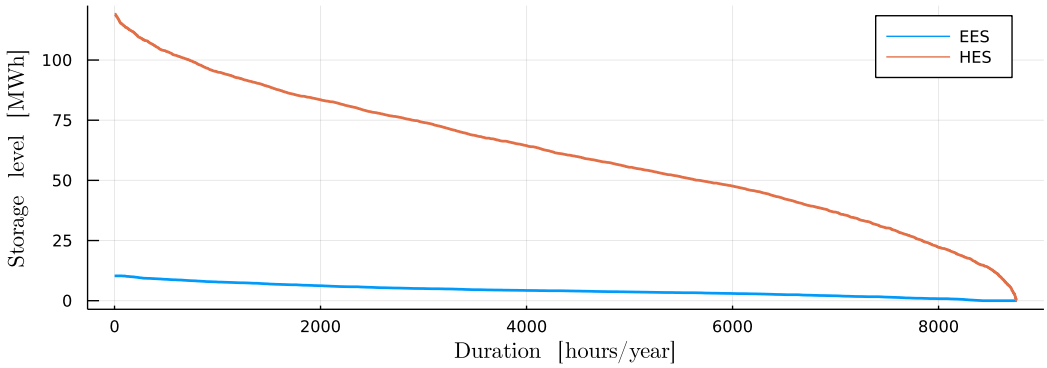

Figure 18: Duration curve of storage levels in case 1.3.

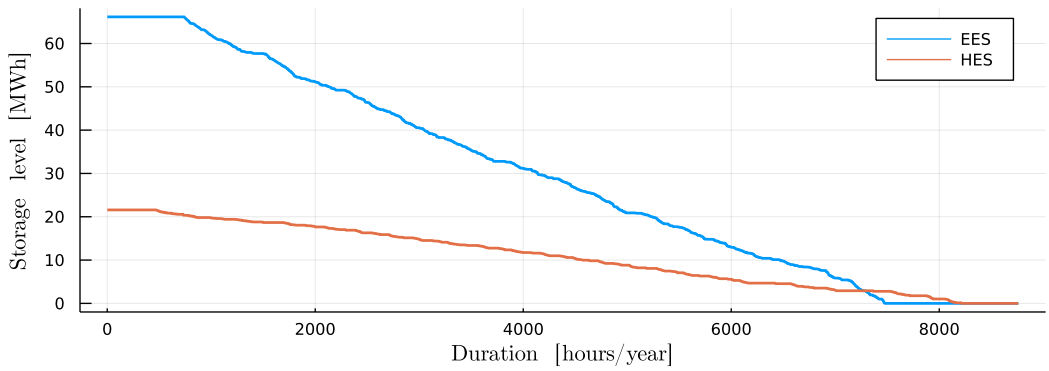

Figure 19: Duration curve of storage levels in case 2.1.

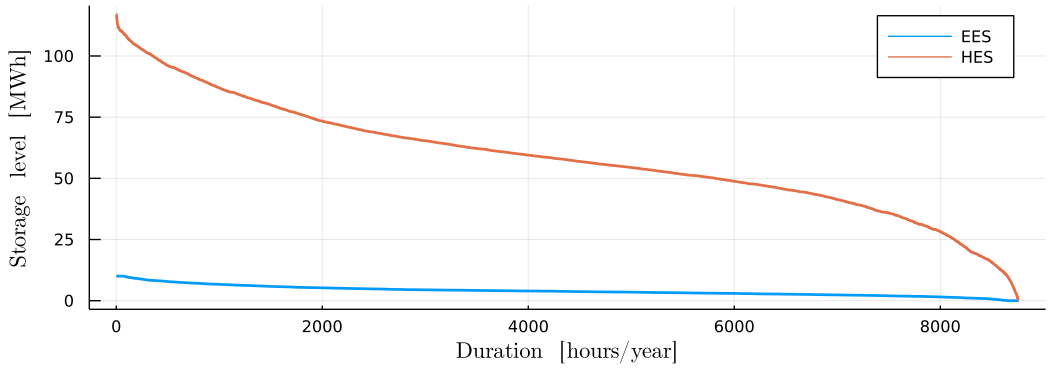

Figure 20: Duration curve of storage levels in case 2.2.

3.3.1 Base case ts

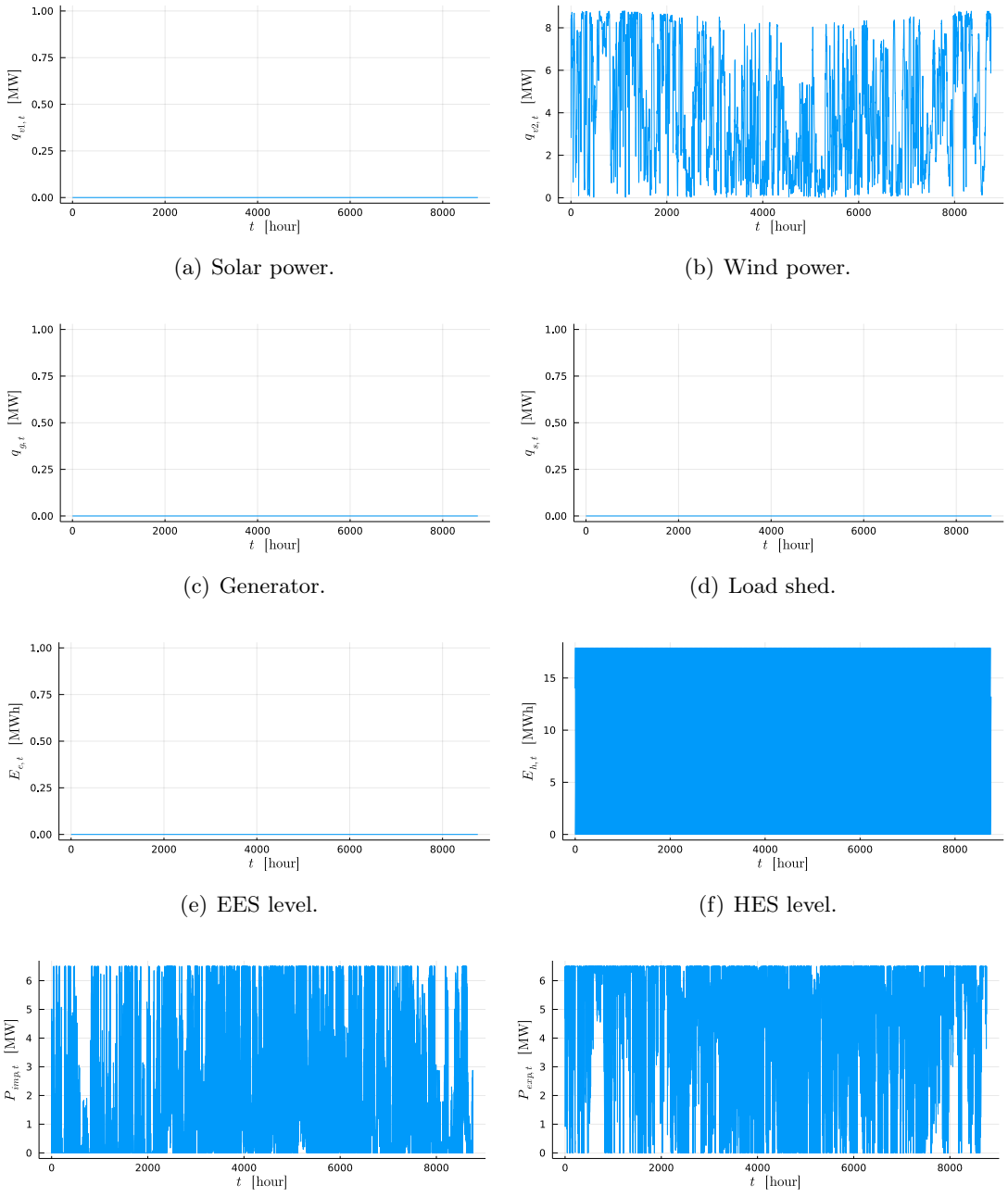

(a) Solar power.

(b) Wind power.

(c) Generator.

(d) Load shed.

(e) EES level.

(f) HES level.

(g) Import powerl.

(h) Export power.

Figure 21: Time series of optimal system scheduling in case 1.1. Production and consumption are given in MW and storage levels are given in MWh.

3.3.2 Isolated system ts

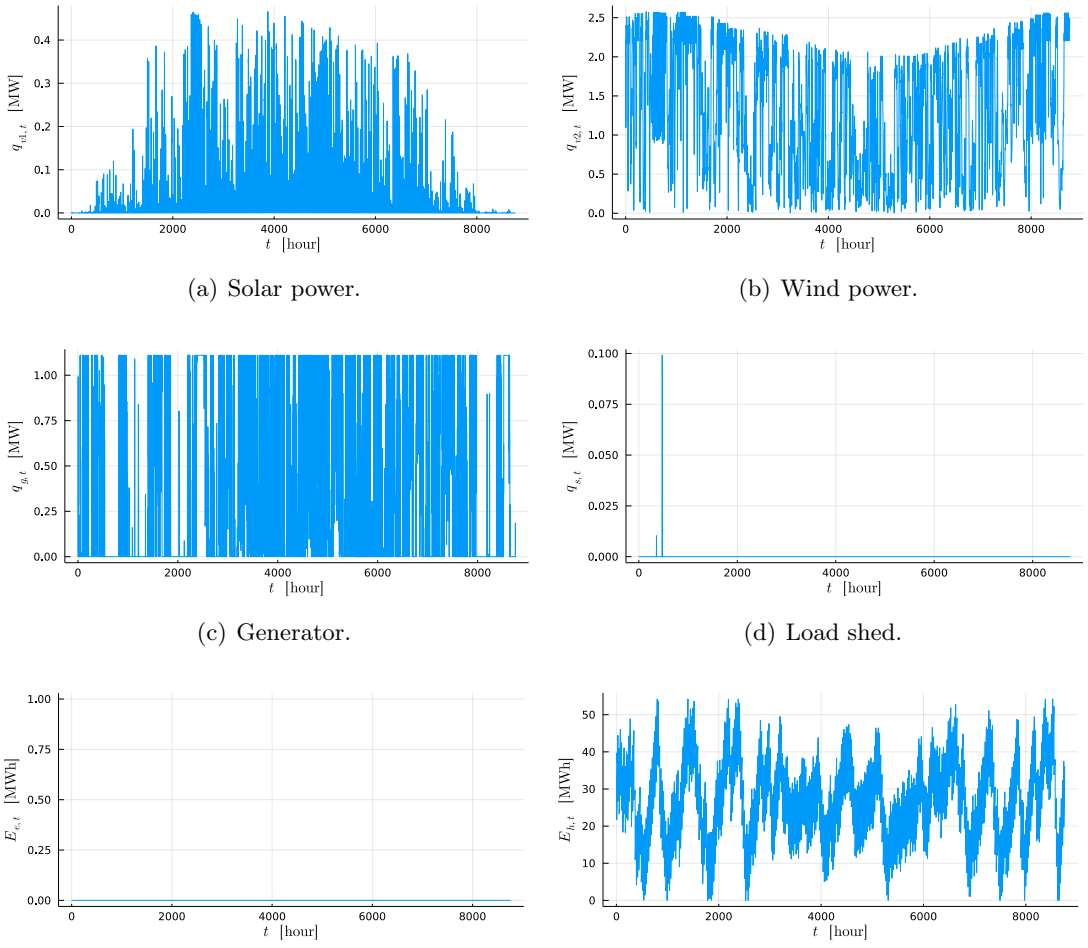

(a) Solar power.

(b) Wind power.

(c) Generator.

(d) Load shed.

(e) EES level.

(f) HES level.

Figure 22: Time series of optimal system scheduling in case 1.2. Production and consumption are given in MW and storage levels are given in MWh.

3.3.3 Fully renewable system ts

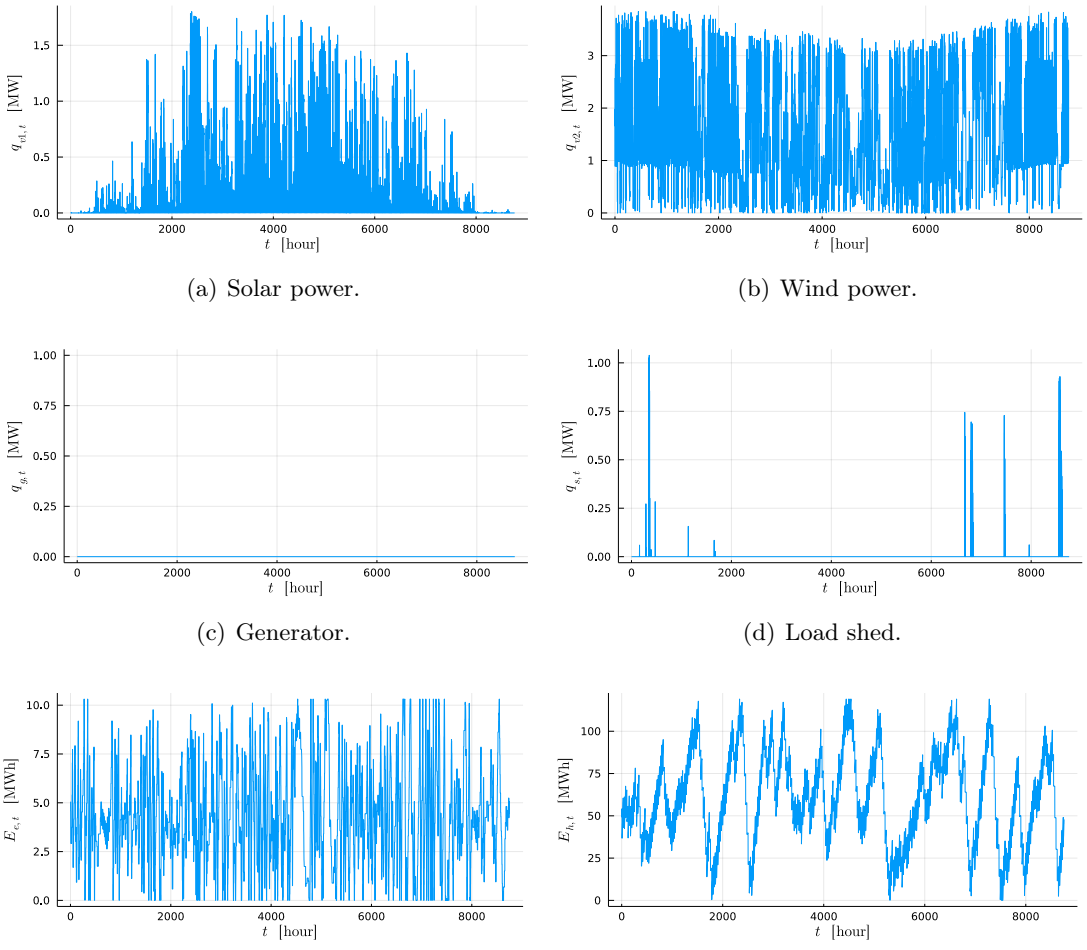

(a) Solar power.

(b) Wind power.

(c) Generator.

(d) Load shed.

(e) EES level.

(f) HES level.

Figure 23: Time series of optimal system scheduling in case 1.3. Production and consumption are given in MW and storage levels are given in MWh.

3.3.4 Replacing wind with solar ts

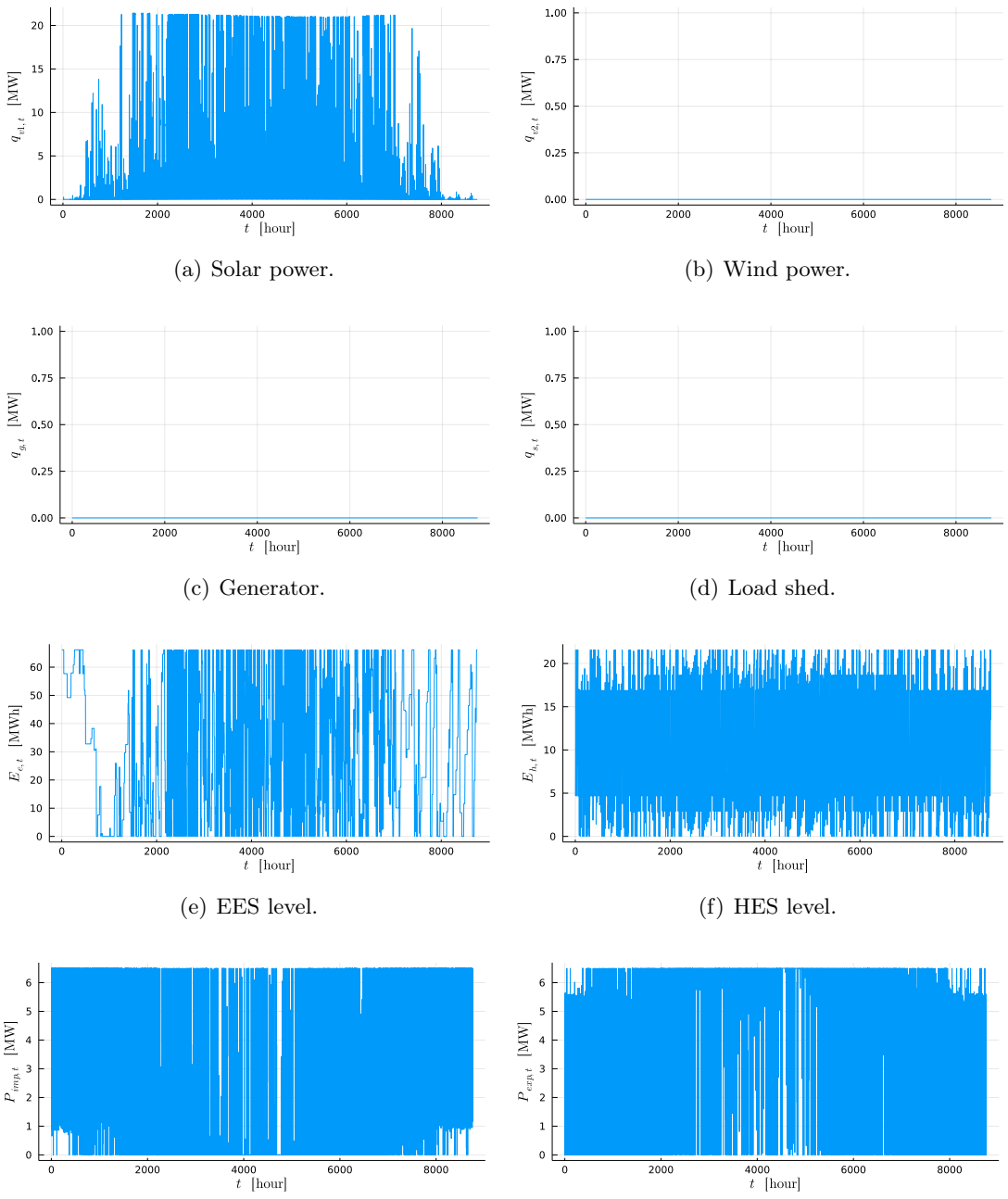

(a) Solar power. (b) Wind power.

(c) Generator. (d) Load shed.

(e) EES level. (f) HES level.

(g) Import power. (h) Export power.

Figure 24: Time series of optimal system scheduling in case 2.1. Production and consumption are given in MW and storage levels are given in MWh.

3.3.5 Fully subsidized solar renewable system ts

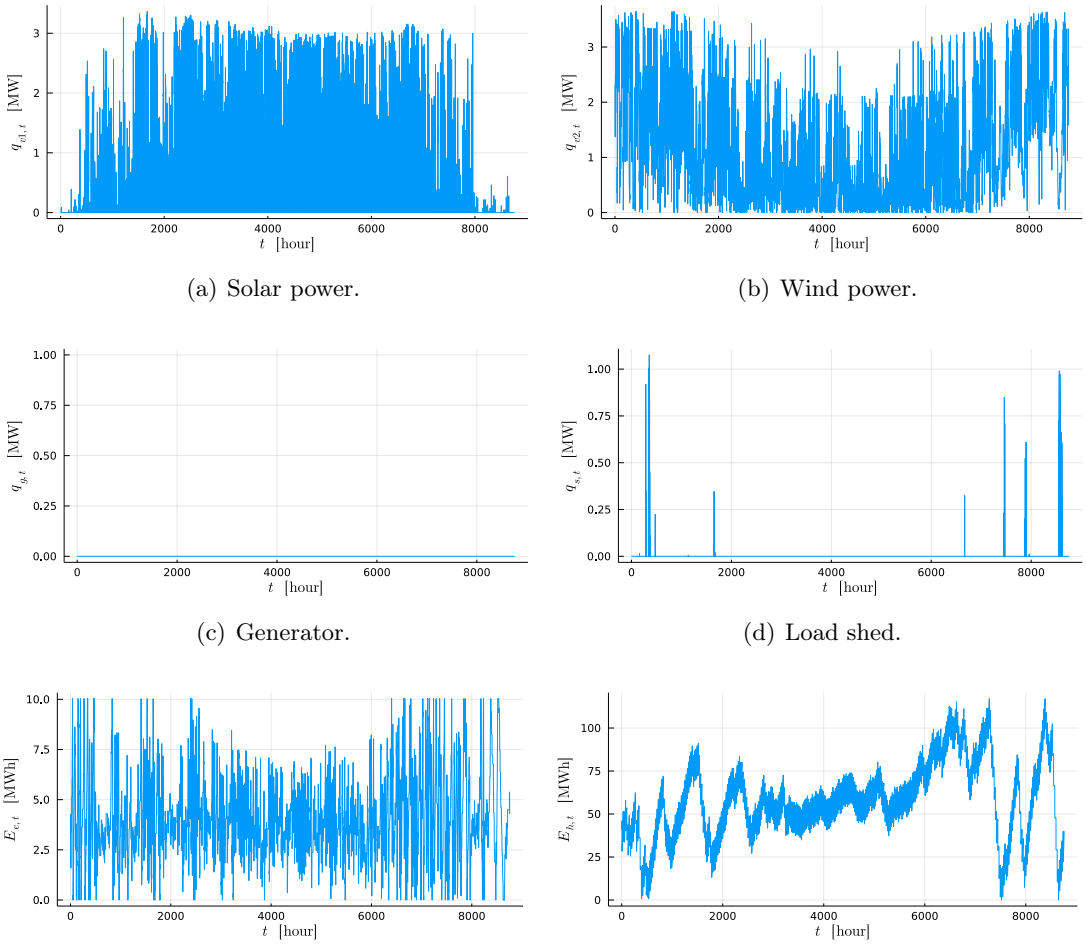

(a) Solar power.

(b) Wind power.

(c) Generator.

(d) Load shed.

(e) EES level.

(f) HES level.

Figure 25: Time series of optimal system scheduling in case 2.2.

3.4 Power flow results

This section contains the results from the power flow calculations. These results consist of annual active power line losses, extreme voltage levels and voltage levels time series. The line losses are presented in section 3.4.1 and the results for bus voltages are presented in section 3.4.2.

3.4.1 Line loss

Table 10 presents the annual line losses for the scheduling provided the CEM. The total line losses are compared with total system generation. Here import power is included in total system generation as this is power injected into the system which causes additional line losses.

Table 10: Line loss for all cases given in GWh and as percentage of total annual system generation.

Case	Line loss [GWh]	Total gen. [GWh]	% of total gen.
1.1	3.80	54.89	6.9
1.2	0.24	16.36	1.5
1.3	0.28	16.54	1.7
2.1	5.50	56.26	9.8
2.1 Rerun	5.02	56.23	8.9
2.2	0.22	16.66	1.3

3.4.2 Bus voltage

Here the bus voltage results from running the PF are presented. Extreme values of peak bus voltages are presented in table 11 and table 12 shows the minimum bus voltages. For each case the extreme voltage is presented as well as both the bus index and the time step the extreme voltage occurred. Thereafter duration curves of bus voltages are plotted in fig. 26-31 to examine how long these extreme voltages occur in the system.

Case 2.1 was the only case to violate the restrictions on bus voltage. Here the voltage levels at multiple buses deviate outside the 15% maximum limit. Additionally, a deviation above 10% lasts for a duration of 350 hours which makes up 4.0 % of the year. As previously stated the voltage levels cannot have 10% deviation for more then 1% of a weekly duration. Therefore the CEM is modified to include additional restrictions on power injection at node 11 in order to maintain voltage stability. The net injection at bus 11 in this case is $P_{11} = P_{v1} - P_{ch} + P_{dch} - P_{eh}$ where P_{v1} is solar plant production, P_{ch} is BESS charging power, P_{dch} is BESS discharge power and P_{eh} is electrolyzer power. The restriction $P_{11} \in \left[-0.5, 10\right]$ MW is implemented and the updated power flow results

Table 11: Peak bus voltage for all cases. Additionally the occurring time step and bus is given.

Case	Voltage [p.u.]	Bus no.	Time step [h]
1.1	1.08	9	5582
1.2	1.00	1	1
1.3	1.01	9	6799
2.1	1.09	9	4840
2.1 rerun	1.09	9	4840
2.2	1.01	9	8573

Table 12: Minimum bus voltage values for all cases. Additionally the occurring time step and bus is given.

Case	Voltage [p.u.]	Bus no.	Time step [h]
1.1	0.95	10	475
1.2	0.96	6	405
1.3	0.96	6	452
2.1	0.81	11	5403
2.1 rerun	0.90	11	8349
2.2	0.96	6	406

for voltage are shown in fig. 30.

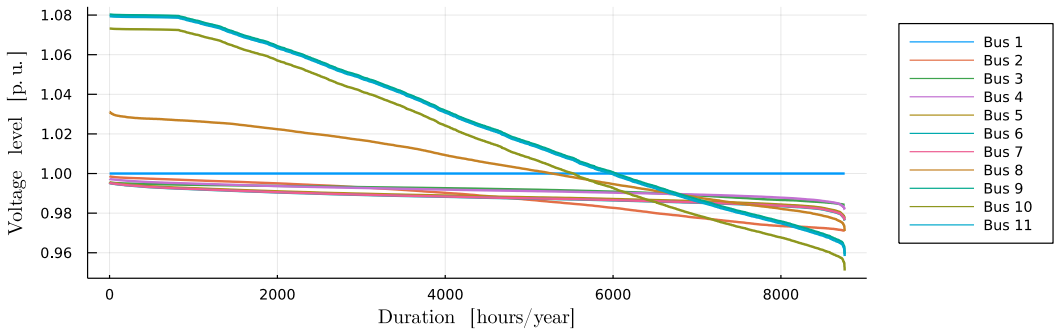

Figure 26: Duration curve of bus voltage for case 1.1.

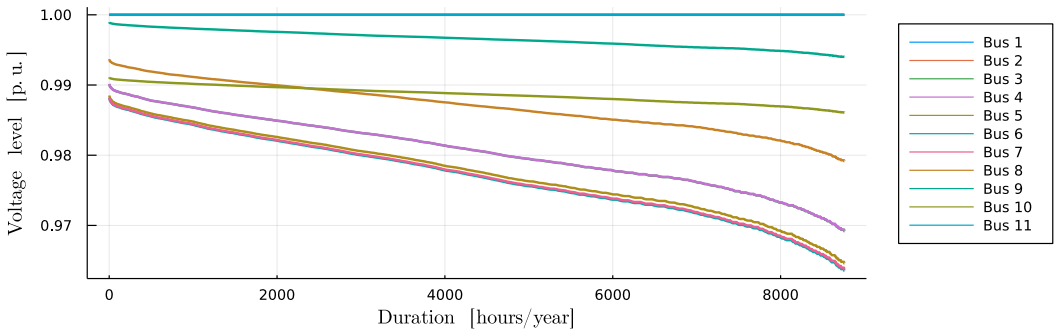

Figure 27: Duration curve of bus voltage for case 1.2.

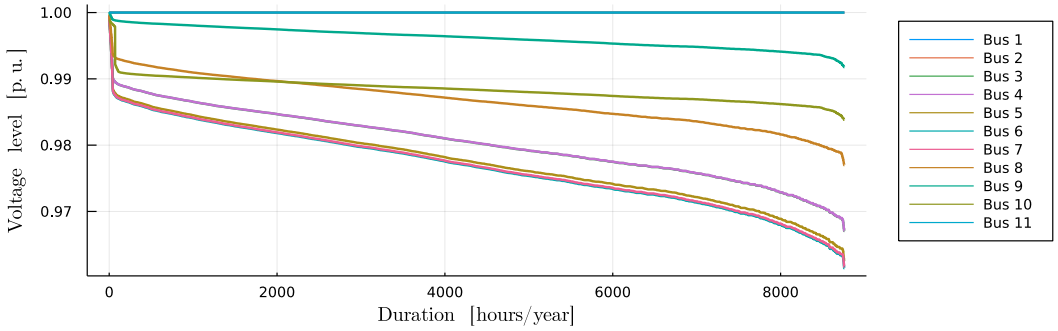

Figure 28: Duration curve of bus voltage for case 1.3.

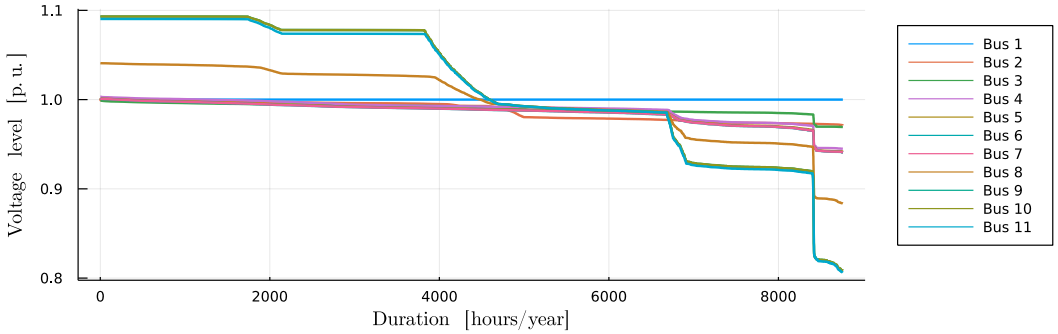

Figure 29: Duration curve of bus voltage for case 2.1.

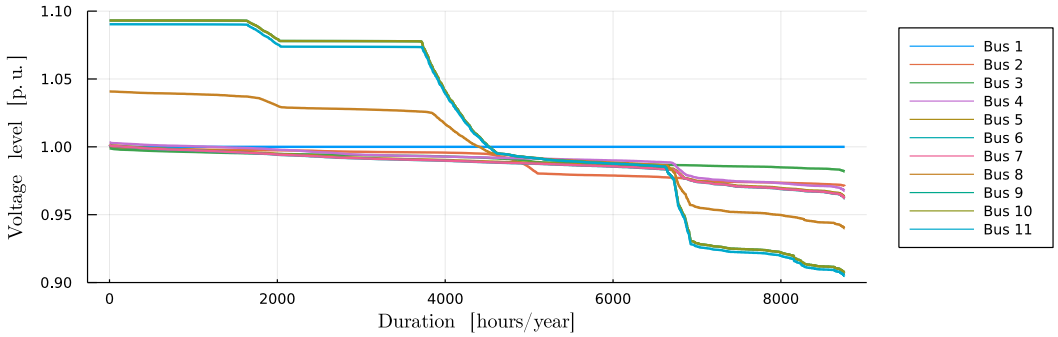

Figure 30: Duration curve of bus voltage for case 2.1 after rerunning the CEM with additional operational constraints.

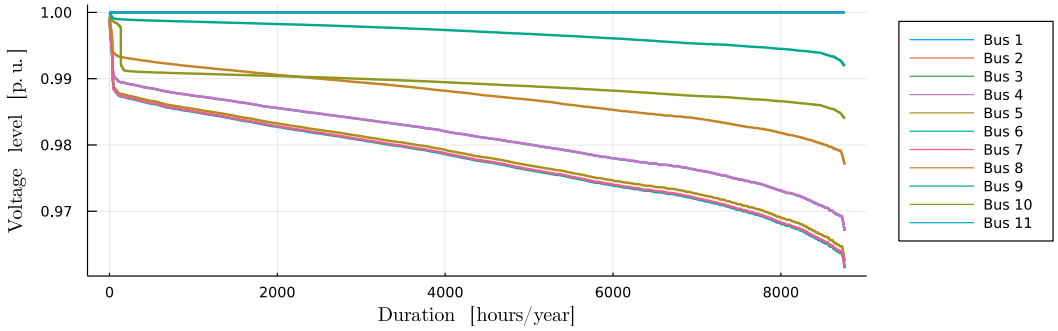

Figure 31: Duration curve of bus voltage for case 2.2.

3.5 Sensitivity analysis

In this section a sensitivity analysis is performed. This is performed by altering one input at a time in order to see how this affects the optimal dimensions of in the system. The sensitivity analysis looks at fuel cell investment cost, solar power availability and wind power availability.

3.5.1 Fuel cell investment cost

A sensitivity analysis is performed on the investment cost of the fuel cell which is altered from 250 to 5500 $/kW in steps of 250 $/kW. The effect this has on optimal system dimensions is shown for case 1.1 and 1.3 in fig. 32 and fig. 33.

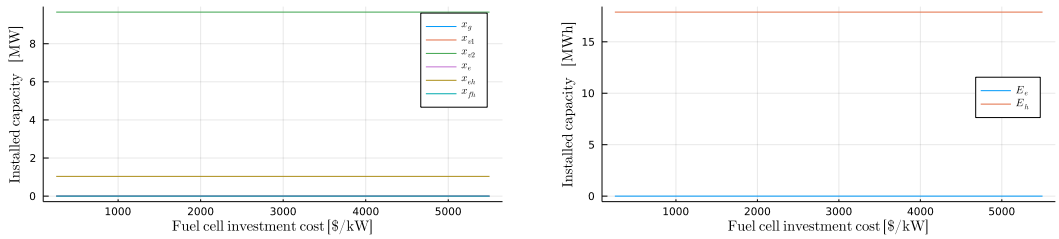

(a) Plant dimensions (b) Storage dimensions

Figure 32: Sensitivity analysis for fuel cell investment cost in case 1.1. Plant dimensions are given in MW and storage capacities in MWh.

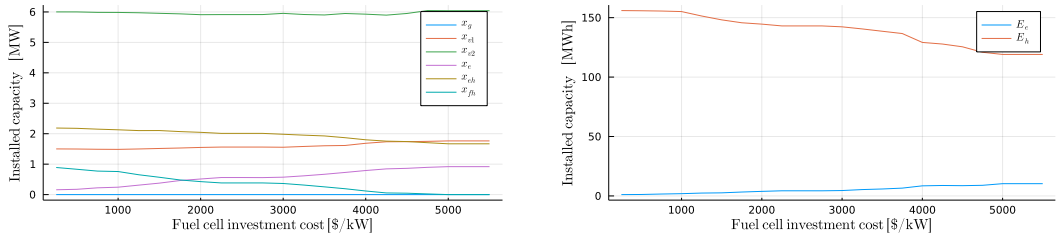

(a) Plant dimensions (b) Storage dimensions

Figure 33: Sensitivity analysis for fuel cell investment cost in case 1.3. Plant dimensions are given in MW and storage capacities in MWh.

3.5.2 Wind power availability

Wind power availability from the years 2010-2019 is collected for Leka similar to the procedure presented in section 2.2.3 [14]. The CEM is optimized for each of these time series for wind power availability and the results are presented for case 1.1 and 1.3 in fig. 34 and fig. 35.

3.5.3 Solar power availability

Data on solar power availability is gathered for the years 2010-2019. The CEM is optimized for these time series for solar power availability while the remaining parameters are kept fixed. The results are shown for case 1.1 and 1.3 in fig. 36 and fig. 37.

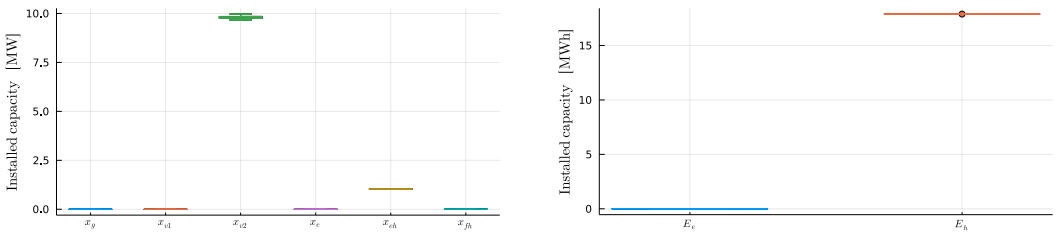

(a) Plant dimensions (b) Storage dimensions

Figure 34: Sensitivity analysis for wind power availability in case 1.1. Plant dimensions are given in MW and storage capacities in MWh.

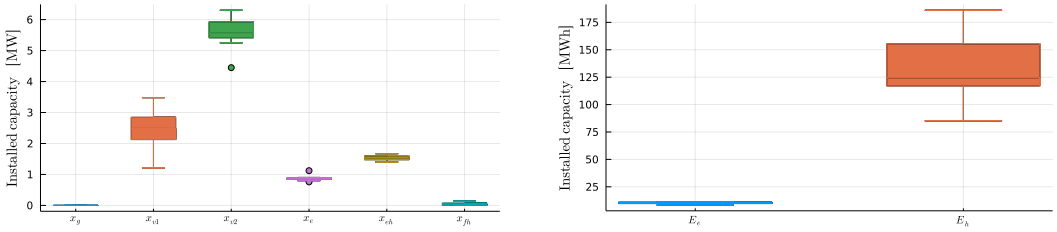

(a) Plant dimensions (b) Storage dimensions

Figure 35: Sensitivity analysis for wind power availability in case 1.3. Plant dimensions are given in MW and storage capacities in MWh.

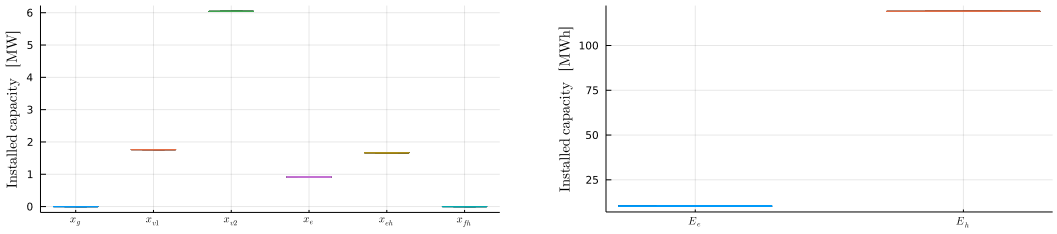

(a) Plant dimensions (b) Storage dimensions

Figure 36: Sensitivity analysis for solar power availability in case 1.1. Plant dimensions are given in MW and storage capacities in MWh.

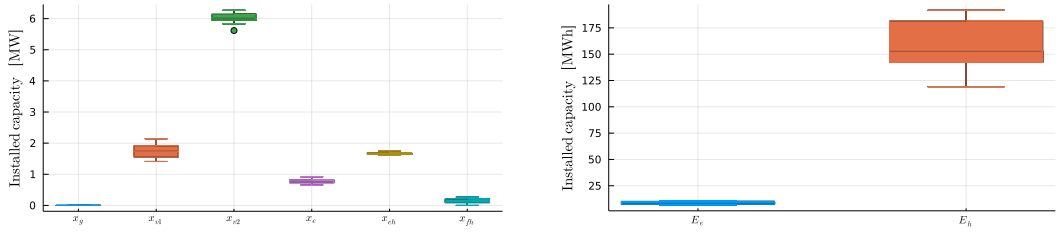

(a) Plant dimensions

(b) Storage dimensions

Figure 37: Sensitivity analysis for solar power availability in case 1.3. Plant dimensions are given in MW and storage capacities in MWh.

4 Analysis of results

In this section, the results provided in section 3 are discussed further, and the different cases are compared. Firstly, the optimal system dimensions and how these affect the annual energy production is examined in section 4.1. The optimal plant and storage scheduling is then discussed in section 4.2. In section 4.3 the system operation is investigated through line losses and bus voltage levels. After that follows a further discussion of how the different systems provide flexibility to cover mismatches in load and generation.

4.1 Optimal system dimensions and energy balance

The optimal system dimensions vary significantly between the different cases as shown in table 6 and 7. These dimensions also impact how the load demand is covered as presented in table 8 and 9. All cases investment in hydrogen storage and an electrolyzer. Hydrogen production through water electrolysis is the only way to cover hydrogen load demand, and the HES capacity reduces the required size of the electrolyzer. The optimal scenario is to invest in the smallest electrolyzer possible and operate it at maximum capacity during the whole year. In order to implement such a solution, there needs to be available power production in every time step, which depends on the type of generation available. These are some of the factors to be discussed in the following cases.

4.1.1 Base case

In case 1.1, the optimal system consists of 9.66 MW installed wind power and an electrolyzer of 1.04 MW capacity. The hydrogen storage required is 17.89 MWh with an initial SoC of 13.22 MWh. The system produces more than double the annual load demand from wind power. Wind power proves to be favoured even though the investment cost is higher than solar power due to the large availability of wind power as presented in fig. 8. The large wind power plant is made profitable through the flexibility provided by the transmission line.

Mismatches in load demand and wind power generation are covered by import and export of power as there is no BESS or fuel cell present to discharge stored energy. The peak electric demand is at most 20% of the transmission capacity. This means load balance can be assured for all time steps even with zero wind power production. Meanwhile, surplus wind power generation is exported to generate additional revenue and reduce the annual costs. The annual specific fixed cost of wind power is \$146.53/kW/yr, which results in an LCOE of 39.1 \$/MWh. This is lower than the spot price for most of the year, as seen in fig. 9, which results in a high incentive to invest in wind power to be utilized for power export. The CEM opts to export at maximum capacity for almost half of the year as seen in fig. 38, which also shows that the net exported power is substantial. Noteworthy, this operation is performed with only 0.45 GWh of wind power curtailment. The high utilization of wind power results in a low annual cost of 0.72 M\$. This results in an energy cost of 44.0 \$/MWh.

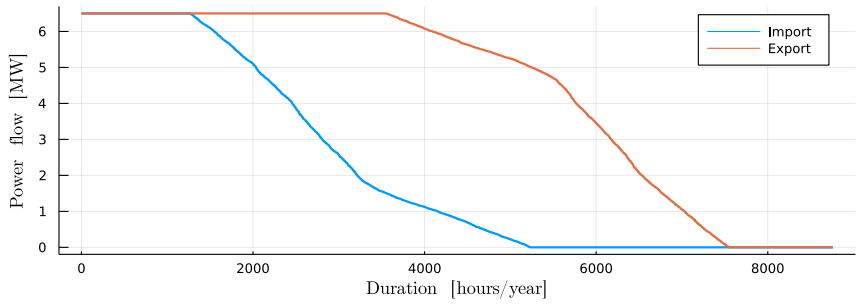

Figure 38: Utilization of the transmission line in case 1.1. In this case there is a net export of 19.86 GWh.

4.1.2 Isolated system

In case 1.2, the possibility for power import and export is removed. The flexibility provided by the transmission line is now replaced by an optimized thermal generator of 1.11 MW capacity. The installed wind power is reduced to 3.72 MW, and an additional 0.45 MW of solar power is added. The electrolyzer is increased by 0.28 MW, and the HES capacity is tripled to 54.22 MWh. On the electric load side, there are now three different power plants instead of only wind power. By investing in both solar and wind power, the risk of not maintaining load balance is lower. The thermal generator can also be dispatched rapidly in order to cover mismatches in load and VRE generation. On the hydrogen side, the flexibility of the transmission line ensured that the HES could be filled on a daily basis, as seen in fig. 21(f). Here, the SoC of the HES varies on a longer time period and is dependant on a larger capacity to ensure the hydrogen load can still be served on days with lower VRE potential.

The isolated system seeks to cover 3.99 of the 16.36 GWh with thermal generation. The wind power plant reduced 61.5% in size, but the annual electricity production is reduced by 67.1 %. The increased VRE curtailment is due to less flexibility in the system. However, even without the transmission line, the optimal system features a renewable share of 75%. In comparison to case 1.1, the annual cost is more than doubled at 1.51 M$, with a energy cost of 92.4 $/MWh.

4.1.3 Fully renewable system

In case 1.3, both the transmission line and the thermal generator is removed. Removing these two sources of flexibility means the CEM now invests in BESS to store surplus VRE production for later use. Both wind and solar power capacity are increased from

case 1.2 to 6.04 MW and 1.76 MW, respectively. The BESS has a capacity of 10.32 MWh and a charging capacity of 0.92MW. The BESS can cover a large share of the electric load as the average electric load demand is 0.82 MW. Again the electrolyzer rating is increased to 1.67 MW, and the HES capacity is more than doubled to 119.05 MWh. This storage can now hold a full six days of hydrogen demand, and this increase is a direct reflection of the lower flexibility present in the system. Due to a lower amount of available generation, the electrolyzer has 2000 hours of downtime, as shown in fig. 39. Therefore the HES capacity needs to be as big to ensure the hydrogen load is met during periods with lower VRE generation. Notably, this system does not need to invest in a fuel cell for extra flexibility even though it already features a sizeable HES capacity.

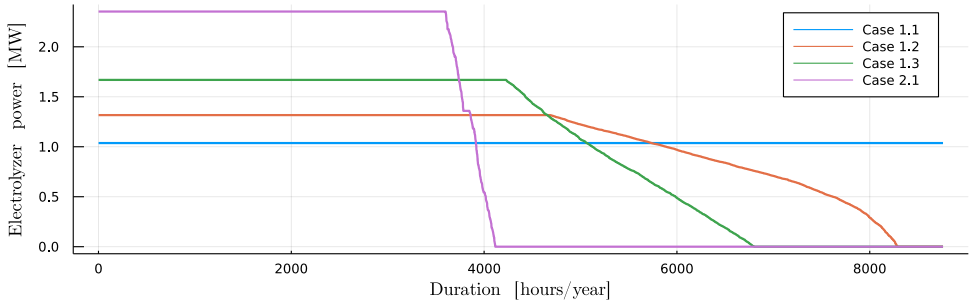

Figure 39: Comparing the capacity and utilization of the electrolyzer in different cases.

In the renewable local energy system, the load demand is covered solely by VRE generation. However, this is the first case to feature some load shedding of 60 MWh. The VRE resources are dependent on sufficient flexibility in order to be fully utilized. In this case, the cost of BESS too high in order to utilize more VRE generation. Due to lacking storage, 8.31 GWh of VRE is curtailed, about 50% of the available VRE. This is a lot higher than the 1.2% curtailment in case 1.1. The increased curtailment results in an annual cost of 2.04 M$ for case 1.3, which is 183% more than in case 1.1, but only 35% more than in case 1.2. The energy cost is now 124.8 $/MWh. In case 1.2 the VRE share of energy production was 75%. As the renewable share reaches 100%, the cost of energy usually follows an exponential growth [7]. However this does not happen in this case where the cost is only increased from 75% to 100%.

4.1.4 Replacing wind with solar

For all the previous cases, wind power has been favoured for bulk energy production. When this option is removed and solar power is set to cover the annual production of wind in case 1.1, the optimal system design is altered drastically and includes 41.40 MW of solar production capacity. Even though this is more than four times the capacity of wind power installed in case 1.1, the new system features a 66.15 MWh BESS with an 11.56 MW discharge capacity. The BESS is quickly emptied at the start of the year and

maintains a high SoC during summer, as can be seen in fig. 24(e). The electrolyzer and HES are both slightly increased at 2.35 MW and 21.58 MWh, respectively. As shown in cases 1.1-1.3, the required electrolyzer power is increased for the lower availability of surplus VRE generation. This is also evident for case 2.1, where the electrolyzer is only operating about half of the year, as shown in fig. 39.

The annual energy production from solar power is 36.21 MWh which equals the wind power production in case 1.1. However, solar power production is concentrated during summer when the electric load demand is low. This mismatch in solar production and load demand causes a phenomenon called the duck curve and can lead to high solar curtailment [19]. Compared to case 1.1, the VRE curtailment is 20 times higher at 8.87 GWh. Compared to solar power, this shows how wind power has a lot more potential in a system located on the Norwegian coastline. By replacing wind power with solar, the annual cost is increased from 0.72 M$ to 5.97 M$. Compared to case 1.1, this translates to a cost increase of 729% to supply the same amount of energy from solar compared to wind power. The cost of energy is now 365.1 $/MWh.

For comparison, removing the energy constraint on solar power, the optimal system would be to invest in no VRE or thermal generation and supply the load demand merely through power import. This yields an annual cost of 1.05 M$. The LCOE of solar power in case 2.1 is 107.6 $/MWh which is a lot higher than the average spot price of 47.38 $/MWh. Solar power availability is also highest when the spot price is lowest. Surplus VRE generation can be exported in case 2.1 as in 1.1, but the power export is not profitable compared to wind power.

Of all the cases, case 2.1 was the only case to violate operational constraints for bus voltage when calculating the power flow. The CEM was then reoptimized by adding additional constraints on power injection at the PV bus (bus 11) within the range $\left[-0.5, 10\right]$ MW. The new optimal system for case 2.1, which now upheld voltage restrictions, shows little difference from the original system. Installed solar power capacity is increased from 41.40 MW to 41.41 MW, and the annual cost is increased from 5.97 to 5.98 M$. The most significant change is that BESS conversion loss is reduced to 3.08 GWh, which is a reduction of 5.5%. However, this reduction merely states that the BESS now has a lower utilization. Overall the optimal system dimensions are little impacted by the added operational constraints.

4.1.5 Fully subsidized solar renewable system

In case 2.2, both the thermal generator and transmission line are removed as in case 1.3. Additionally, the investment- and operation cost of solar power is set to 1 $/kW and 1 $/kWh in order for solar to replace wind power. However, this does not seem to be the case as the optimal system design features both solar and wind power plants. As compared to case 1.3, the solar plant is increased from 1.76 MW to 34.78 MW. Even though the solar plant is practically free, wind power availability is so good that the optimal

size of wind power is here 4.67 MW compared to 6.04 MW in case 1.3. The remaining components are similarly sized and slightly smaller for BESS and HES as there is more VRE generation available to cover the load.

The fact that the CEM still chooses to invest in wind power when solar power is free is unexpected. The annual production from solar power is only increased from 1.57 GWh to 6.3 GWh even though the installed capacity of solar power is increased by 20 times. The wind plant produces 10.36 GWh annually, a decrease of 30.7%, which has been shifted to the solar plant. The annual specific fixed cost (ASFC) of wind power is 146.5 $/kW and 1.1 $/kW for solar power. Using these ASFCs, the LCOE values for solar and wind power generation are 5.95 $/MWh and 66.1 $/MWh respectively. Solar power is a lot cheaper, but to be utilized in periods outside of solar generation, the power has to be stored in either BESS or HES and converted back to electrical power. As there is no option for power export, the surplus solar power cannot be utilized as a solution including a fuel cell and increased BESS capacity is more expensive than wind power. By reducing the ASFC of solar by 99.0%, the annual operation costs of 1.68 M$ feature only a 17.6% decrease. This represents an energy cost of 102.8 $/MWh.

4.1.6 Summary of optimal system dimensions

The optimal system dimensions show that wind power production is heavily favoured in the Leka system. This is due to the larger availability of wind energy which follows the same seasonal variation as the electric load demand. In order to utilize solar power to the same degree as wind power, additional flexibility in terms of storage is needed.

In the more constrained cases, the annual costs increase drastically. This is largely due to energy storage costing a lot more than VRE production capacity. The 100% renewable, isolated system costs three times as much as the base case and two times as much as simply covering load demand through power import.

The large transmission line provides much flexibility for VRE production. This lets the model over-dimension VRE production to cover the load as the surplus generation is exported for profit. In case 1.1, the LCOE of wind power is lower than the spot price most of the year and wind power utilization is only limited by the transmission cable capacity. With a larger transmission line, the optimal investment of wind power would increase and the annual costs would be reduced even further.

4.2 Optimal system scheduling

Here the optimal system scheduling and production variations within a year are analyzed. The optimal system scheduling as presented in section 3.3.1 - 3.3.5 show interesting differences in scheduling between the different cases. Some of these time series have already been mentioned, but this subsection analyses further the duration curves of both plant

production and storage levels for the different cases given in fig. 11-15 and fig. 16-20. By examining the whole system as a single node, power generation is shown as positive power injection and power consumption is shown as negative power injection.

4.2.1 Plant production

The duration curves of power injection show some key differences in optimal scheduling for the different cases. For duration curves, it is most interesting to examine the peak scheduling as this often determines the limits of the system. Additionally, the VRE production scheduling duration features some interesting differences.

For cases 1.1-1.3, the scheduling is similarly distributed even though the systems feature components of vastly different sizes. In case 1.2, the annual production is a lot lower as export is removed from negative power injection (curves below zero) in fig. 12. Case 1.3 features a higher peak utilization of wind and solar compared to cases 1.1 and 1.2. This is most likely due to the added BESS that provides additional flexibility to handle peak VRE production.

In case 2, the scheduling is quite different from case 1. Instead of a peak, the solar power production in case 2.1 starts with a plateau of 700 hours above 20 MW, before fading out after 4000 hours. Additionally, the BESS is now scheduled to cover peak demand for 70 hours, while the total utilization time of the BESS is similar to case 1.3. VRE generation in case 2.2 has a small peak before flattening out for the first 2000 hours. Here the peak VRE generation may be able to be stored in the BESS for later use rather than being curtailed as in case 2.1

Common for all cases is that the peak VRE production is lower than the installed capacity. For example, in case 1.1 there is 9.66 MW of installed wind power, but the peak wind production is only 8.79 MW, as seen in fig. 11. Comparing the peak scheduled VRE power productions to the installed capacity for each case yields the results in table 13 for the wind power plants and table 14 for the solar plants. In other words, peak power production is not utilized in all cases except the solar plants in cases 1.2 and 1.3. These plants are small, and both cases feature a larger wind plant that has unused peak production.

The reason for this over-dimensioning of VRE plants is due to the intermittent availability. These plants cannot be regulated, and power production is related to the availability of certain weather conditions. Doubling the size of a VRE plant guarantees the same production even though the availability is halved. After a certain amount of VRE production is installed, adding additional capacity will not increase the peak VRE production, as can be seen by the plateau of solar power in fig. 14. However, additional VRE capacity can provide a larger production from hours with lower availability, and the annual energy production is increased. The CEM decides to over-dimension the VRE plants as it is

cheaper to curtail a part of the peak VRE production than invest in energy storage.

Table 13: Comparison of peak wind power scheduling and installed wind power capacity.

Case	Peak wind prod. [MW]	Installed cap. [MW]	Unused peak prod. [%]
Case 1.1	8.79	9.66	9.0
Case 1.2	2.58	3.72	30.7
Case 1.3	3.84	6.04	36.4
Case 2.1	0	0	-
Case 2.2	3.65	4.67	21.9

In table 13 case 1.3 features the largest wind power over-dimensioning of 36.4%. The same table shows that peak VRE production is better utilized in cases that feature flexibility as a transmission cable or energy storage. In table 14 case 2.1 features 48.2% unused peak VRE production and case 2.2 has 90.3%. Due to the lower availability of solar power, the solar plants feature a significantly larger over-dimensioning.

Table 14: Comparison of peak solar power scheduling and installed solar power capacity.

Case	Peak solar prod. [MW]	Installed cap. [MW]	Unused peak prod. [%]
Case 1.1	0	0	-
Case 1.2	0.45	0.45	0
Case 1.3	1.76	1.76	0
Case 2.1	21.45	41.40	48.2
Case 2.2	3.37	34.78	90.3

4.2.2 Storage levels

The duration curves of the storage levels in fig. 16-20 show some interesting results of BESS and HES scheduling. First of all, the HES in case 1.1 sticks out as it contains 24 steps rather than a smooth curve, as seen in fig. 16. These steps are caused by constant electrolyzer scheduling. The HES is emptied at 06-07 each morning. Each hour until 06 the next day, the HES level is increased by one hour of electrolyzer production.

Cases 1.2, 1.3 and 2.2 have similar HES scheduling as these cases all feature a wind power plant as shown in fig. 22(f), 23(f) and fig. 25(f). In these cases, the HES is larger and fills up over time as surplus wind power generation is utilized for water electrolysis. The HES capacity for these cases is a lot larger than in case 1.1. This increase is caused by a lack of predictable power supply, which is unable to convert 18.66 MWh of hydrogen per

day. The HES, therefore, requires a buffer that represents the variations in wind power availability. Case 1.2 follows the same scheduling as cases 1.3 and 2.2, but this system contains a thermal generator that provides flexible power generation, and therefore the HES is smaller in this case.

Case 2.1 is different from the others as it features a large BESS and a HES of similar size to case 1.1. Here the transmission line provides the flexibility to convert the daily hydrogen demand each day reliably. However, the large solar plant introduces a demand for a BESS. This find is similar to the results from the project thesis regarding high solar penetration [6]. The cost of HES capacity is only 1452 $/MWh, and the added flexibility increases the use of solar power for electrolysis rather than imported power that costs 47.38 $/MWh on average. However, the most exciting part of case 2.1 is the scheduling of the large BESS. This storage is quickly discharged during the first two months (about 1500 hours) of the year. As the solar power production increases, the BESS starts to fill up gradually and even reaches maximum capacity for 700 hours of the year during months of high solar power production. The large BESS is expensive, but provides the flexibility needed to utilize solar power to a more considerable degree.

4.3 System operation analysis

System operation is evaluated on transmission losses and bus voltage stability. The previously modelled 1-bus system is now modelled as an 11-node system with internal transmission lines, each with a respective impedance value as previously presented. The line losses are a function of impedance multiplied by current squared and feature large differences between cases with and without external transmission. Bus voltage levels are determined by the load flow equations. Firstly the total system line losses are presented in section 4.3.1 and the voltage stability analysis is presented in section 4.3.2.

4.3.1 Line loss

The total line losses result from solving the load flow problem for all 8760 hours using the CEM scheduling as the input for power injections and load. As previously mentioned, the CEM does not take line losses into account, and therefore the optimal scheduling is optimistic. It features rapid changes in power production, import and export as there are no drawbacks that limit the CEM from such scheduling. These flaws are highlighted by the PF results.

The line losses show a clear tendency where the systems that utilize import and export feature line losses 12-20 times the line losses in cases without external grid transmission. In cases 1.1 and 2.1, the line losses are as high as 3.80 GWh and 5.50 GWh. These losses equal 6.9% and 9.8% of the total system generation in these cases. These losses are large because of the high utilization of the transmission line. The VRE plants are located at

buses 10 and 11, which means the exported power needs to flow through lines 10/11-9, 9-8, 8-4, 4-3, 3-2 and transformer 2-1 before it reaches the external grid. All these lines have line losses as a function of current squared which adds up. Additionally, imported power might have to be transferred back to supply the electrolyzer at bus 11. The energy could be more efficiently utilized if it were not transferred back and forth from the external grid.

In cases 1.2, 1.3 and 2.2 the line losses are only 0.24, 0.28 and 0.22 GWh, equalling 1.5%, 1.7% and 1.3% of total power generation. These cases feature lower losses due to the scheduled power flows being much smaller than in cases 1.1 and 2.1. Case 2.2 has the lowest line losses of all the cases. This could result from the solar plant being located at bus 11, where it can supply the electrolyzer without any transmission loss. However, the differences in line losses for these cases are small and could be due to other factors.

An interesting result is that when case 2.1 is rerun with additional operational constraints, the line losses are reduced by 0.48 GWh. This equals a reduction of 8.7% by slightly altering the scheduled production. The resulting power flows are flatter, which again reduces the line losses in case 2.1.

The energy lost in transmission would have to be covered by additional power generation to meet the load demand. However, this is not included in the CEM, and extending the CEM formulation to take line losses into account would change the optimal system dimensions and the optimal scheduling. However, a transmission loss of 10% would yield an LCOE for wind power of approximately 43.4 $/MWh in case 1.1. That is still enough to ensure high wind power investment, but the margins for profit are smaller based on the average spot price of 47.38 $/MWh.

4.3.2 Voltage stability

Similarly to the results on line loss, the voltage results show a clear difference between the cases with transmission and the cases without transmission. For cases 1.2, 1.3 and 2.2, the transmission line is removed, and bus 11 is chosen as the swing/slack bus. The voltage level at this bus is set to 1.0 p.u. as defined in section 1.3. As the power injection in the system is concentrated close to bus 11, the duration curves fig. 27, 28 and fig. 31 therefore show few voltage levels above 1.0 p.u. In cases 1.1 and 2.1, the slack bus is located in node 1, and these cases then feature higher voltage levels in the system during export and lower voltage levels during import as seen in fig. 26 and fig. 29. Case 2.1 was the only case to violate the voltage restrictions and is therefore analyzed in greater detail than the other cases.

In case 1.1, the peak voltage is 1.08, while the minimum voltage is 0.95. The voltage level deviates most at bus 9 and 11 while bus 10 follows close behind. These are located furthest away from the slack bus and close to the bus with wind power production. The system is operated at the highest deviation for about 700 hours but remains well inside

the 10% restriction limit. Bus 8 follows a similar trend but has overall less of a deviation. The remaining buses do not deviate more than 2% from the rated values. Therefore the optimal system for case 1.1 does not violate the restrictions on voltage levels.

In cases 1.2, 1.3 and 2.2, there is little variation in bus voltage levels. In these cases, the power injections within the system are small compared to the cases utilizing power export, and thus the voltage levels are kept within 0.96-1.00 p.u. There are some small differences within the first few hours of the duration curves, but this is most likely due to the different system dimensions in these cases. A reason for the minor deviations in these cases could be the location of the slack bus. The electrolyzer is also located on bus 11, which means the electrolyzer can be supplied without affecting the voltage levels at other buses. Perhaps the bus voltages would be more affected if the slack bus was located in another bus. In general, the small load demand leads to lower power flows and lower variations in bus voltages.

Case 2.1 features the largest variations in bus voltage as seen in fig. 29. The peak bus voltage is 1.09 p.u. and the minimum voltage is as low as 0.81 p.u. These are both located at bus 11 and result from positive and negative power injection in this bus. At bus 11, the duration curve shows a high voltage level of about 4000 hours which is about the same number of hours the solar plant is producing as seen in fig. 14. The final 1500 hours show the lowest voltage level as 0.95, and the final 350 hours are below the restriction level of 0.9. These minima are caused by too low power injection at bus 11, which occurs when 11.56 MW BESS charging is scheduled during low solar generation. The power supplying BESS charging is transferred from bus 1, which causes issues with too low voltage on bus 11. Therefore case 2.1 was reoptimized with limitations on net power injection on bus 11.

The new power flow results for node voltages are shown in the duration curve in fig. 29. Additionally, the time series of bus voltages at buses 9, 10 and 11 are compared in fig. 40. Here the most drastic dips below 0.9 p.u. are now removed. However, some of the peaks above 1.0 p.u. are also removed, which might indicate that the restrictions added were too strict, or this could be the CEM spreading out scheduled power production which it did not have constraints for before. The added operational constraints on net injection at bus 11 do not change the optimal system dimensions but merely alter the optimal system scheduling. The scheduling of BESS charging is given in fig. 41. This now features a lower utilization of peak BESS charging, which can lead to voltage stability challenges in bus 11.

The optimal system in case 2.1 features an over-dimensioned solar plant that produces more than twice the total energy demand in the system. Integrating large amounts of solar power can lead to stability issues due to the solar production pattern. Solar production is highly concentrated at noon when the load demand is low. In the evening solar production fades to zero, while the load demand increases as in fig. 5(b). This imbalance causes a phenomenon called the duck curve, which is one of the most important challenges in integrating large scale solar power production [19]. The voltage levels during a

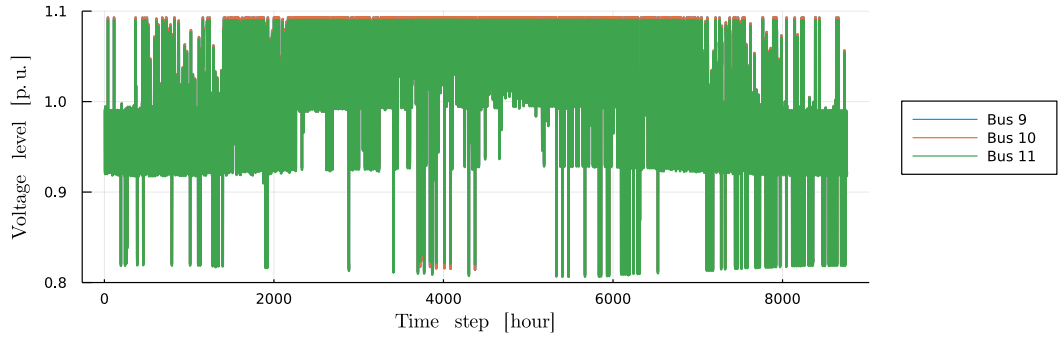

(a) Before additional operation constraints.

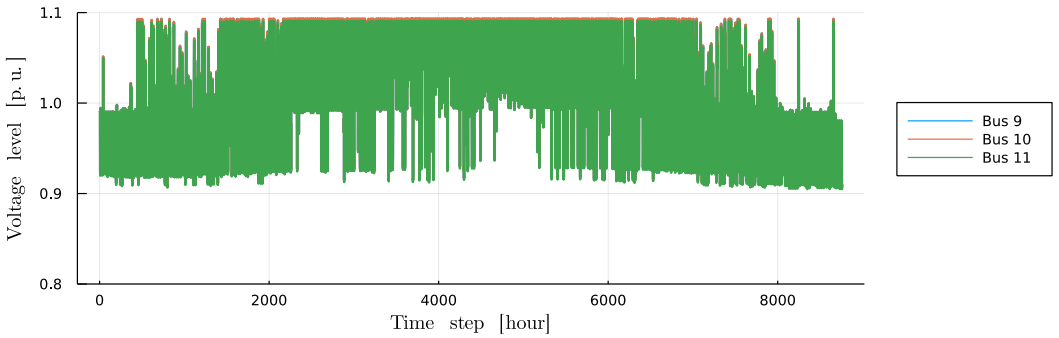

(b) After additional operation constraints.

Figure 40: Comparison of bus voltages on bus 9, 10 and 11 before and after case 2.1 is optimized with added operational constraints.

day where the net load follows the duck curve are given in fig. 42. The duck curve must be smoothed out using energy storage, demand-side flexibility or by curtailing part of the solar production. In case 2.1, a rather large BESS is present to help smooth out the duck curve and provide the most stable operation possible.

4.3.3 Summary of operation analysis

In this system, the cases with external transmission capacity feature the highest line losses and the most significant deviation in bus voltage levels. However, the wind system in case 1.1 featured operation just barely within the feasible limit on bus voltage. Case 2.1 violated the voltage restrictions. A rescheduling of charging and discharging from the BESS was required to operate within adequate limits on bus voltage.

Cases 1.1 and 2.1 feature system operation within the defined voltage restrictions. However, these cases are close to the 10% limit, and further calculations are required to

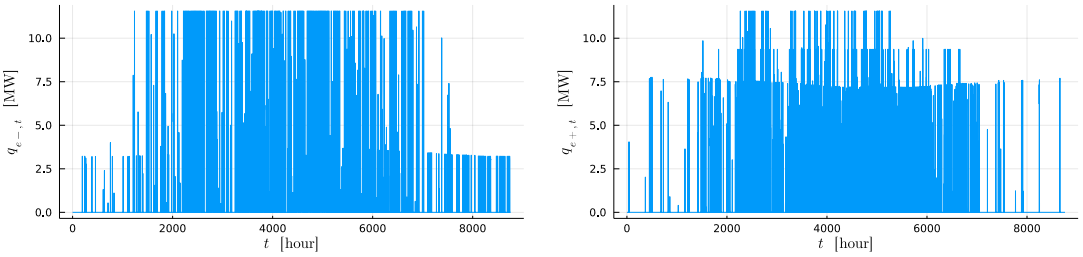

(a) Before (b) After

Figure 41: EES charging power ($q_{e-,t}$) scheduling before and after additional operational constraints were added to case 2.1.

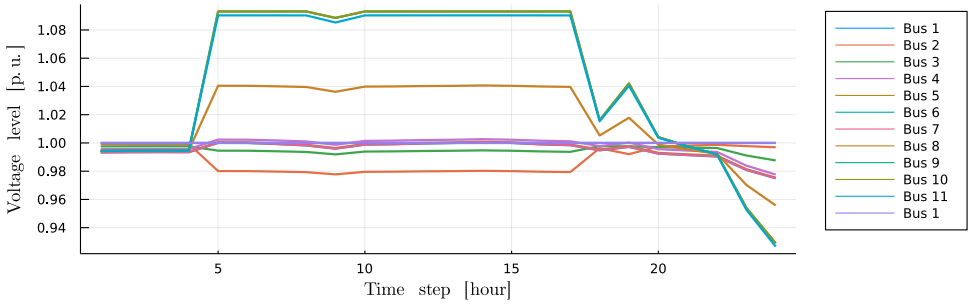

Figure 42: Voltage levels as a result of net load following the duck curve for a single day.

guarantee voltage stability for these cases.

A weakness of the CEM scheduling is that it is often jagged rather than smooth. Large and rapid changes in power injection can lead to infeasible voltage levels and high line losses. By reoptimizing the CEM scheduling, the line losses were reduced by 8.7% without altering the system dimensions. This is due to the characteristics of power lines where losses are a function of the current squared.

4.4 Sensitivity analysis

4.4.1 Fuel cell investment cost

The initial value of fuel cell investment cost is 5425.34 $/kW and is too high to activate the fuel cell investment in any of the cases. The fuel cell could convert hydrogen back to electrical power in hours with low VRE production or cover peak load, but this comes at the cost of high conversion loss. With an efficiency of 0.55 for the fuel cell, the roundtrip efficiency of the hydrogen loop becomes 0.41. However, if the system features high VRE curtailment, much of the energy would be lost either way. The sensitivity

of fuel cell investment cost is examined for case 1.1 and 1.3 as shown in fig. 32 and fig. 33.

As seen in fig. 32 changing the investment cost of the fuel cell causes no change in optimal system dimensioning. The high utilization of external grid transmission provides enough flexibility to cause very little VRE curtailment. Therefore the low roundtrip efficiency is too low to utilize a fuel cell cost-effectively for case 1.1. Case 1.3, on the other hand, features higher VRE curtailment as both the thermal generator and the transmission line is removed.

In fig. 33 the fuel cell investment is now activated. When the investment cost of the fuel cell is low enough, the HES replaces the BESS almost entirely. For lower BESS capacity, the installed PV is also lower, which was also the case in the project thesis submitted last December [6]. Additionally, the electrolyzer capacity is slightly higher to keep up with the larger utilization of hydrogen. When the investment cost of the fuel cell is 250 $/kW (4.6% of the original value), the objective value is 1.88 M$, which is a 7.8% decrease. Additionally, the curtailed VRE is reduced to 7.14 GWh, a decrease of 14.1%. This scenario is not realistic with such a low cost of the fuel cell, but sensitivity analysis shows how the fuel cell can benefit from large portions of surplus VRE generation, which is otherwise curtailed.

4.4.2 Wind power availability

Wind power availability is intermittent, and the actual production from wind power in a given hour is difficult to forecast. Historical weather data can be used to give a decently good approximation. Wind power availability from 2010-2019 is collected similarly to the procedure presented in section 2.2.3 [14]. The CEM is optimized for each of these time series and the results are presented for case 1.1 and 1.3 in fig. 34 and fig. 35.

In case 1.1, there is little variation in optimal system dimensions when the wind power availability is altered. This is likely due to the transmission line providing enough flexibility to cover mismatches in load balance. There is a small variation in the installed wind power capacity of 0.30 MW which is 3.1 % of the average installed capacity.

In case 1.3, there are more significant variations compared to case 1.1. As this is a 100% renewable stand-alone system, there is a greater demand for flexibility. The difference in wind power availability causes a 41.2% variation in wind power capacity and 33.1% variation in solar power capacity. None of the cases feature low enough wind power availability to install in a thermal generator. However, the largest variation is seen to be in the HES capacity. The smallest HES is 85.15 MWh and can cover four days of hydrogen demand without additional hydrogen conversion. The largest HES is 186.1 MWh which can cover almost ten days of hydrogen demand at full capacity. In a renewable stand-alone system where the only buffer is HES capacity, this should be over-dimensioned to some extent as further uncertainties could occur. For example, if one of the wind turbines would

malfunction, there would not be enough power generation to meet the load demand. A possible extension of this thesis could be a contingency analysis. This could be done on both generators and transmission lines to examine the effects this might have on optimal system dimensions and operation.

4.4.3 Solar power availability

Similarly to wind power, data on solar power availability was gathered, and the results are shown for cases 1.1 and 1.3 in fig. 36 and fig. 37.

In case 1.1, there is zero variation in optimal system dimensions based on solar availability. This case originally featured no solar power, and there is not a single year with good enough solar availability to activate the solar power investment. In case 1.3 there are some variations similar to fig. 35. The solar plant was originally smaller in this case and had lower annual energy production. Therefore the optimal dimensions vary less when solar power is altered. Another reason for a lower impact of solar power variation is that solar power follows a diurnal pattern as shown in fig. 43. Some days might have larger peak production, but the solar production is always zero at night, making solar power more predictable for half of the daily hours. On the other hand, wind power is more intermittent and will therefore lead to larger variations in optimal system dimensions.

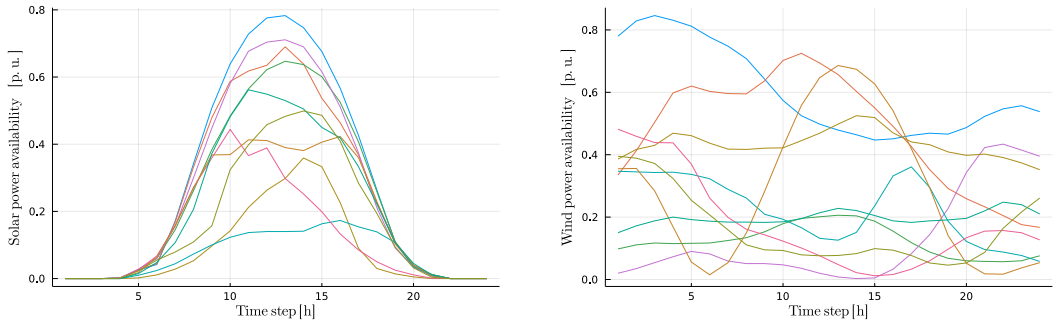

(a) Solar (b) Wind

Figure 43: VRE availability for an arbitrary summer day in p.u. for 10 different years.

4.5 Sources of error

In the results presented above there some inaccuracies. The real world is chaotic and hard to model 100% accurately. Therefore assumptions are made in order to simplify certain aspects in order to make a system description fit within the formulation of a

model. Some key sources of error are presented below.

4.5.1 Input data

The input data of load demand and VRE availability are given in an hourly resolution. In reality these represent the average values of variations within each hour. It is therefore likely that the peak load demand and VRE availability are larger. Also the act of balancing load and demand on a smaller time scale would be even more challenging, possibly requiring more flexibility in order to utilize VRE to the same extent.

However, the time scale of one hour was chosen in order to overall potential of VRE integration. However, it should be noted that hours featuring operation close to the restrictions should be examined closer, possibly also on a shorter time scale in order to get more precise results of power system operation.

4.5.2 Component operation and degradation

The CEM assumes constant efficiency for components like the thermal generator, the electrolyzer, EES charge/discharge and fuel cell. This is a simplification as the efficiency of components can vary based on multiple different factors like temperature, loading and age. For example, both the SoC and the performance of EES operation can vary based on temperature [20] [21]. Additionally components degrade over time, leading to lower efficiencies [22] [23]. However the models would quickly become advanced if all these considerations were added, and therefore the simplifications are made.

4.5.3 Model limitations

The CEM is formulated as an LP and thus an optimal solution is guaranteed. However, this deterministic solution is optimistic and does not represent a realistic scenario. However this does function as a theoretical upper limit to the optimal system dimensions. This could be compared to other stochastic models featuring more realistic results to see how large the differences in annual cost or grid losses are.

The optimal scheduling is jagged, which causes challenges in system operation. This could be improved by adding some form of grid loss constraint. The grid losses are quadratic (RI^2), but this could be implemented as a approximated as a piecewise linear function in order to maintain the linear structure of the CEM.

5 Conclusion

In this thesis, the operation of a combined electricity-hydrogen system has been analyzed for optimal system designs featuring high renewable penetration. The optimal system dimensions were optimized by implementing and solving a least-cost capacity expansion model. The optimal hourly scheduling of plants and storages were analyzed from an operational standpoint by calculating grid losses and bus voltage levels using AC power flow. The optimal system design, scheduling and operation were then compared for different scenarios in a case study of the Norwegian island Leka. At Leka there is limited transfer capacity to the external grid and the option of implementing a hydrogen powered ferry is examined.

In this case study, the results feature different optimal systems favouring wind power investments due to the large availability of wind energy and a low LCOE of 39.1 $/MWh. With an average spot price of 47.38 $/MWh used in the case study, the wind plant is dimensioned to maximize power export and is only limited by the capacity of the transmission cable connecting Leka to the external power grid. In the wind system, power import is used to cover mismatches in wind generation and load demand. As the wind generation is jagged and unpredictable, so is the demand for import and export power. These rapidly changing power flows lead to total grid losses that equal 23.2% of the total load demand. However, this jagged scheduling of wind power causes a maximum deviation of 8% in bus voltage, so the scheduling features a viable system operation.

When wind power is replaced by solar power with equal average power generation, the annual system operation cost is increased five times. This increase is due to the lower availability of solar power and the costly BESS required to avoid the curtailment of surplus solar generation. Here the high utilization of import and export also lead to large grid losses. The scheduling of BESS charging caused the bus voltage to drop by 19% for a 4% duration of the year. As this violated the voltage restrictions, the CEM was reoptimized with additional operation constraints on power injection. The new optimal system featured similar system dimensions, but the scheduling was distributed more evenly. The BESS charging followed solar production closer, which resulted in valid system operation and a reduction in grid losses of 8.7%. Even if the cost of solar power was fully subsidized, the least-cost system included a significant amount of wind power. This fact shows how superior the availability of wind power is in coastal regions in Norway.

One set of cases was formulated to examine the effects of removing certain types of flexibility. Firstly the transmission line was removed which caused a 56.8% reduction in VRE capacity. However VRE production now included solar power and still covered 75% of the total energy demand. The remainder was covered by a thermal generator. Without the transmission line the annual system operation cost was doubled. Thereafter, the thermal generator was also removed. This activated the EES investment as well as some load shedding. Additionally, the capacity of both VRE plants were now increased in

order to serve peak demand previously covered by the thermal generator. However, this lead to four times as much VRE curtailment. The capacity of the HES in these cases also reflected the removal of flexibility, as the capacity was increased from 1, to 3, to 6 days of hydrogen load demand. For the fully renewable system the annual costs were increased by 183% compared to the base case, and 35% compared to the system with thermal generation. This is a rather small increase for increasing the share of renewable energy production from 75% to 100%.

The different case studies highlighted that the external transmission line most beneficial source of flexibility for VRE integration. Surplus VRE generation can be utilized through power export to generate revenue, and power import can provide backup in periods when VRE generation is low. Other types of flexibility utilized were EES and HES. EES was only utilized in combination with solar power and the solar only case featured a BESS with 66.15 MWh capacity. On the other side, HES was present in every system due to the hydrogen load. However, the HES capacity varied significantly based on the buffer required to cover the hydrogen demand in periods with low VRE production. The size of the HES varied from one day to six days of storage, which is a lot lower than for the logistic model that did not feature optimal sizing [1].

In the Leka power system, the transmission capacity to the external grid was five times as large as the peak electric load demand. Such a large transmission line provides much flexibility for over-dimensioning the VRE plants. However, if scheduled sub-optimally, the large variations in power injection can lead to voltage issues. Therefore, it is vital to plan the scheduling of VRE generation, storage charging, and discharging to uphold all limits on system operation.

6 Further work

During the work on this thesis, some interesting ideas for further development were uncovered. The possible extensions of this work could provide light on unanswered questions outside the scope of this thesis. The most exciting extensions are presented below:

- Further analysis of voltage levels. In this thesis, there are example systems with scheduling that feature voltage levels close to the limits for a considerable portion of the year. Therefore, a more extensive analysis of the voltage levels is required. A better solution to plant scheduling could be made utilizing optimal power flow (OPF).
- The methodology in fig. 4 could be implemented using OPF rather than PF. Here the main difference is that the OPF only takes generator capacity as input and not generator production. This method could remove the drawback of using the CEM production schedules, which proved to be jagged as there are no limits on line losses. The OPF is then able to provide generator scheduling that takes line losses into account. The OPF outputs the cost of operation for each time step, and this cost could be compared to the annual cost provided by the CEM.
- Contingency analysis could be incorporated in the PF calculations. In this formulation of the CEM, both scheduled and unscheduled downtime of generators not examined. This is unrealistic as removing the generator for some duration of the year will cause a demand for additional flexibility. A contingency analysis could also be performed on transmission lines.
- The CEM could be expanded to include the option of grid investments. In the base case, VRE integration was limited by the transmission capacity. If the transmission capacity were larger, more VRE could be integrated into the system. For some cases, the VRE availability might be so great that it might be beneficial to invest in additional transmission capacity to increase export revenue [24].
- As also mentioned in the project thesis, demand-side flexibility is an interesting topic that could be further investigated. The intermittent VRE availability could pair well in a power system where mismatches in load and generation are tolerated to some extent. This thesis has shown that VRE sources can provide more than enough energy in a year. The challenge, however, is to produce it at the right time. End users could, for example, be paid directly for shifting their load. This load shifting could show a lower use of shedding and VRE curtailment.

References

[1] Korpaas M, Greiner CJ, Holen AT. A logistic model for assessment of wind power combined with electrolytic hydrogen production in weak grids. In: 15th Power Systems Computation Conference, PSCC 2005; 2005. .

[2] Horowitz CA. Paris Agreement. International Legal Materials. 2016;55(4).

[3] Bouckaert S, Araceli Fernandez Pales CM, Remme U. Net Zero by 2050: A Roadmap for the Global Energy Sector; 2021.

[4] Olje- og energidepartementet, Klima og miljødepartementet. Regjeringens hydrogenstrategi på vei mot lavutslippssamfunnet; 2020. .

[5] Aarskog FG, Danebergs J, Strømgren T, Ulleberg Ø. Energy and cost analysis of a hydrogen driven high speed passenger ferry. International Shipbuilding Progress. 2019;67:97–123. Available from: https://content.iospress.com/articles/international-shipbuilding-progress/isp190273.

[6] Bjørnerem ES. Optimal dimensioning of isolated, renewable hydrogen systems for integrating wind and solar power.; 2020. .

[7] Greiner CJ. Sizing and Operation of Wind-Hydrogen Energy Systems. Norwegian University of Science and Technology; 2010.

[8] Strbac G. Demand side management: Benefits and challenges. Energy Policy. 2008;36 (12):4419–4426. Available from: https://doi.org/10.1016/j.enpol.2008.09.030.

[9] Korpås M, Botterud A. Optimality Conditions and Cost Recovery in Electricity Markets with Variable Renewable Energy and Energy Storage. MIT CEEPR Working Papers 2020-005. March 2020. Available from: http://ceepr.mit.edu/publications/working-papers/721.

[10] Zimmerman RD, Murillo-Sánchez CE, Thomas RJ. MATPOWER: Steady-state operations, planning, and analysis tools for power systems research and education. IEEE Transactions on Power Systems. 2011;26(1).

[11] Masetti C. Revision of European Standard EN 50160 on power quality: Reasons and solutions. In: ICHQP 2010 - 14th International Conference on Harmonics and Quality of Power; 2010. .

[12] Office of Energy Efficiency and Renewable Energy (EERE). Hydrogen Storage; 2021. Available from: https://www.energy.gov/eere/fuelcells/hydrogen-storage.

[13] Eichman J, Townsend A, Melaina M. Economic Assessment of Hydrogen Technologies Participating in California Electricity Markets. National Renewable Energy Laboratory. 2016. Available from: https://www.nrel.gov/docs/fy16osti/65856.pdf.

[14] Pfenninger S, Staffell I. Renewables.ninja [Internet]; 2016. Available from: https://www.renewables.ninja/about.

[15] Pfenninger S, Staffell I. Long-term patterns of European PV output using 30 years of validated hourly reanalysis and satellite data. Energy. 2016;114:1251–1265. Available from: https://doi.org/10.1016/j.energy.2016.08.060.

[16] Staffell I, Pfenninger S. Using Bias-Corrected Reanalysis to Simulate Current and Future Wind Power Output. Energy. 2016;114:1224–1239. Available from: https://doi.org/10.1016/j.energy.2016.08.068.

[17] Nord Pool. Historical Market Data; 2021. Available from: https://www.nordpoolgroup.com/historical-market-data/.

[18] Dunning I, Huchette J, Lubin M. JuMP: A modeling language for mathematical optimization. SIAM Review. 2017;59(2).

[19] Wang Q, Chang P, Bai R, Liu W, Dai J, Tang Y. Mitigation strategy for duck curve in high photovoltaic penetration power system using concentrating solar power station. Energies. 2019;12(18).

[20] Waldmann T, Wilka M, Kasper M, Fleischhammer M, Wohlfahrt-Mehrens M. Temperature dependent ageing mechanisms in Lithium-ion batteries - A Post-Mortem study. Journal of Power Sources. 2014;262.

[21] Lu Z, Yu XL, Wei LC, Cao F, Zhang LY, Meng XZ, et al. A comprehensive experimental study on temperature-dependent performance of lithium-ion battery. Applied Thermal Engineering. 2019;158.

[22] Jia X, Jin C, Buzza M, Wang W, Lee J. Wind turbine performance degradation assessment based on a novel similarity metric for machine performance curves. Renewable Energy. 2016;99.

[23] Jørgensen M, Norrman K, Krebs FC. Stability/degradation of polymer solar cells; 2008.

[24] Trötscher T, Korpås M. A framework to determine optimal offshore grid structures for wind power integration and power exchange. Wind Energy. 2011;14(8).

[25] Norges vassdrags- og energidirektorat (NVE). Dokumentasjon for kostnadar i energisektoren [Internet]; 2019. Available from: https://www.nve.no/energiforsyning/energiforsyningsdata/dokumentasjon-for-kostnadar-i-energisektoren/.

[26] De Vita A, Kielichowska I, Mandatowa P. Technology pathways in decarbonisation scenarios. EU-ASSET Project Deliverable. 2018.

[27] Bødal EF, Mallapragada D, Botterud A, Korpås M. Decarbonization synergies from joint planning of electricity and hydrogen production: A Texas case study. International Journal of Hydrogen Energy. 2020;45(58):32899–32915. Available from: https://www.sciencedirect.com/science/article/pii/S0360319920335679.

[28] Cole WJ, Frazier A. Cost Projections for Utility-Scale Battery Storage. National Renewable Energy Laboratory. 2019. Available from: https://https://www.nrel.gov/docs/fy19osti/73222.pdf.

Appendix

A Input parameters for CEM

Table 15: Input parameters for plant costs to be used in the CEM.

Parameter	Cost	Unit	Description
r	0.06	-	Discout rate [25]
V_s	3000	\$/MWh	Shedding cost [9]
SCC_g	934	\$/kW	Specific capital cost of generator [26]
$OM_{g,fixed}$	35.64	\$/(kW year)	Fixed O&M costs of generator [25]
L_g	30	year	Lifetime of generator [25]
c_{fuel}	21.285	\$/MWh fuel	Fuel cost of generator [25]
η_g	0.26	-	Generator efficiency [25]
c_{CO2}	30	\$/ton CO2	CO2 price [27]
e_g	0.18	ton/MWh fuel	CO2-content of fuel [9]
$OM_{g,var}$	1.73	\$/MWh	Variable O&M costs of generator [25]
SCC_{v1}	865.2	\$/kWp	Specific capital cost of solar power [26]
$OM_{v1,fixed}$	15.18	\$/(kW year)	Fixed O&M costs of solar power [25]
L_{v1}	25.00	year	Lifetime of solar power [25]
SCC_{v2}	1674.0	\$/kW	Specific capital cost of wind power [26]
$OM_{v2,fixed}$	14.3	\$/(kW year)	Fixed O&M costs of wind power [25]
L_{v2}	25	year	Lifetime of wind power [25]
SCC_e^{pwr}	680.0	\$/kW	Investment cost of power interface to EES [28]
L_e^{pwr}	15	year	Lifetime of power interface to EES [28]
SCC_e^{en}	210.0	\$/kWh	Investment cost of energy storage [28]
L_en	15	year	Lifetime of energy storage [28]
η_{e-}	0.9	-	Charging efficiency [28]
η_{e+}	0.9	-	Discharging efficiency [28]
SCC_{eh}	1708	\$/kW	Specific capital cost of electrolyzer [13]
$OM_{eh,fixed}$	59.78	\$/(kW year)	Fixed O&M costs of electrolyzer [13]
L_{eh}	15	year	Lifetime of electrolyzer [13]
η_{eh}	0.75	-	Electrolyzer efficiency [13]
SCC_{fh}	5425.34	\$/kW	Specific capital cost of fuel cell [13]
$OM_{fh,fixed}$	81.74	\$/(kW year)	Fixed O&M costs of fuel cell [13]
L_fh	15	year	Lifetime of fuel cell [13]
η_{fh}	0.55	-	Fuel cell efficiency [13]
SCC_h^{en}	20	\$/kWh	Investment cost HES [27]
L_h	30	year	Lifetime of HES [27]

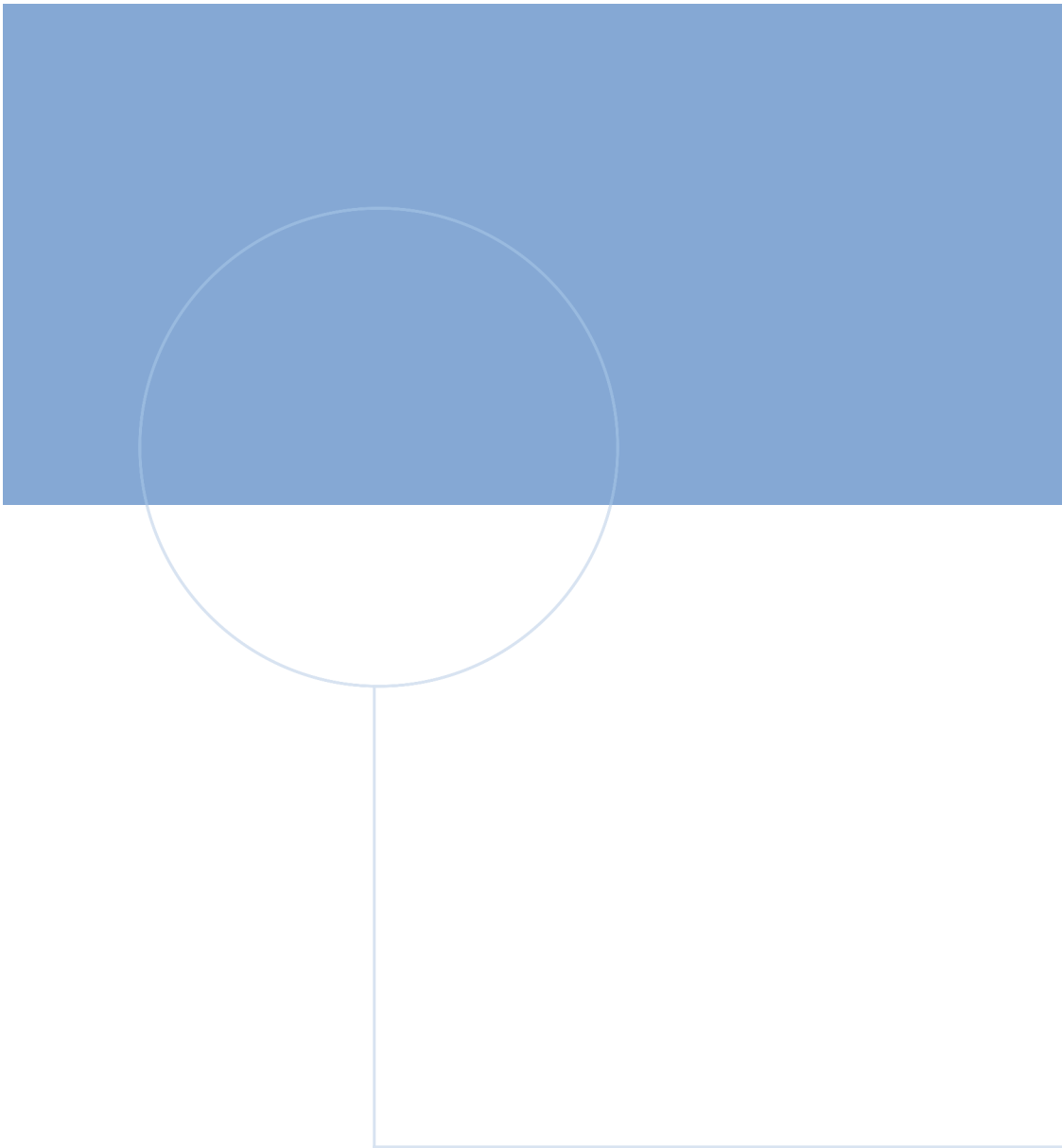

NTNU

Norwegian University of
Science and Technology